frontiers in Earth Science

ORIGINAL RESEARCH
published: 29 March 2021
doi: 10.3389/feart.2021.631405

Structural Significance of the Mid-level Décollement Within the Western Sichuan Fold-And-Thrust Belt (WSFTB), Insights From Sandbox Modeling

Chuang Sun [1,2], Zhigang Li [1,2]*, Shimin Wu [1,2], Zhiyuan He [3], Shaotian Zhao [1] and Panfei Wang [1]*

[1]Guangdong Provincial Key Lab of Geodynamics and Geohazards, School of Earth Sciences and Engineering, Sun Yat-Sen University, Guangzhou, China, [2]Southern Marine Science and Engineering Guangdong Laboratory, Zhuhai, China, [3]Laboratory for Mineralogy and Petrology, Department of Geology, Ghent University, Ghent, Belgium

The *WSFTB* is located outboard of the eastern Tibetan Plateau, western China. It has received great attention due to high earthquake risks and rich resources of oil and gas. For both issues, the detailed structural configuration and deformation mechanism behind it are of great importance, but remain unclear due to the complexity created by the presence of multiple décollements. The effect of regionally distributed shallow Triassic salt décollement (SD) and the basal one (BD) has been well understood. In this paper, we focus on the third décollement situated between them. We conducted three sandbox experiments by varying this mid-level décollement (MD) from absence to presence, and from frictional to viscous, to test the effect on diversity of regional structural configuration. Our experimental results illustrated that 1) Absence of MD facilitated decoupling on SD, forming the greatest contrast between subsurface deformation front and the blind one beneath SD; 2) Frictional MD itself showed little decoupling, while its weakness reduced the bulk strength of deep structural level, lowering decoupling effect on SD and leading to approximating deformation fronts in the shallow and deep; 3) The viscous MD, along with SD relieved the resistance on their interbed layer. Consequently, the fastest deformation propagation rate and farthest deformation front (in all the experiments) occurred in the middle structural level. The modeled fold and thrust structures are comparable with the southern, central and northern *WSFTB* respectively, suggesting that varied MD may control the along-strike structural variations presented. The results also indicate that MD can alter the deformation partition in depth of any other multiple décollement system.

Keywords: Sichuan Basin, fold and thrust belt, multiple décollements, sandbox modeling, the Longmen Shan fault belt

OPEN ACCESS

Edited by:
Gang Rao,
Zhejiang University, China

Reviewed by:
Dan-Ping Yan,
China University of Geosciences, China
Oliver Duffy,
University of Texas at Austin, United States

****Correspondence:***
Chuang Sun
sunchuang@mail.sysu.edu.cn
Zhigang Li
lizhigang@mail.sysu.edu.cn

Specialty section:
This article was submitted to Structural Geology and Tectonics, a section of the journal Frontiers in Earth Science

Received: *20 November 2020*
Accepted: *08 February 2021*
Published: *29 March 2021*

Citation:
Sun C, Li Z, Wu S, He Z, Zhao S and Wang P (2021) Structural Significance of the Mid-level Décollement Within the Western Sichuan Fold-And-Thrust Belt (WSFTB), Insights From Sandbox Modeling. Front. Earth Sci. 9:631405. doi: 10.3389/feart.2021.631405

1. INTRODUCTION

The western Sichuan fold and thrust belt (*WSFTB*) extends the front of Longmen Shan mountain (**Figure 1**), standing as an extremely important target for oil and gas exploration, and a region of high seismicity. It is the first natural gas exploiting area in China and has long been considered a prime area for natural gas exploration owing to the presence of abundant source-reservoir-cap rocks, (e.g.

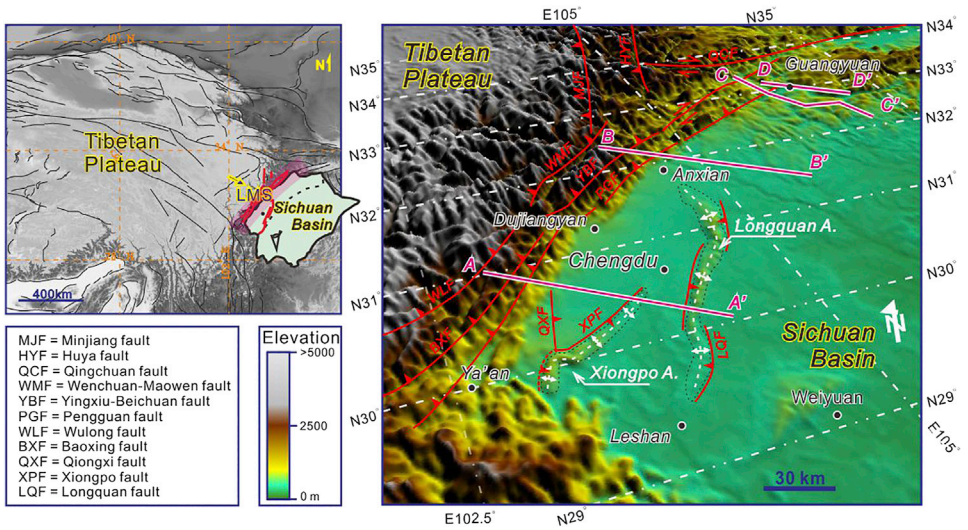

FIGURE 1 | Morphological features in the western Sichuan (an oblique view). The pink lines indicated the locations of four cross sections in **Figure 2**, roughly. *A.* indicates anticline; LMS, Longmen Shan.

Jia et al., 2006; Tang et al., 2008; Liu et al., 2012; Zou et al., 2015; Gong et al., 2015; Li et al., 2019a; Chen et al., 2019). Recently, a historic discovery was made in the northern segment of the *WSFTB*, a giant gas field with a maximum daily output of $220 \times 10^4\ m^3$ was found in a blind structure named Shuangyushi. This confirms previous exploring prospects and indicates huge potential in similar structures. On the other hand, the *WSFTB* is still under active shortening in response to eastward growth of the Tibetan Plateau (Wang et al., 2013a; Wang et al., 2013b; Li et al., 2016; Li et al., 2017; Wang and Lin, 2017; Li et al., 2019c; Jia et al., 2020). Its deformation front (the Longquan anticline) is seismically active and may be responsible for the 1967 Ms5.5 Renshou earthquake (Wang and Lin, 2017). While in the Frontier of Longmen Shan (the transition zone between the Longmen Shan orogen and the *WSFTB*), several blind structures exist, these include the range front fault, (e.g. Hubbard et al., 2010; Li et al., 2014; Li et al., 2016; Li et al., 2017) and the Hongya blind fault (Wang et al., 2014a). These faults represent deformation migration in the deep, and also exert significant seismic hazards to the densely populated Chengdu Plain as illustrated by the 1970 M_s6.2 Dayi earthquake and the 2013 M_w6.6 Lushan earthquake (Li et al., 2016).

To assess both potential size of gas and oil reservoir and the possible maximum co-seismic rupture, an understanding of the structures bearing them (especially the structural continuity along the strike and dip) is clearly issue of significant importance. The *WSFTB* striking ~500 km long in the NE-direction (**Figure 1**) is characterized by along-strike segmentation and decoupling in deep. In its southern segment (south of Dujiangyan), the superficial structures are isolated anticlines detached by the shallower Triassic salt décollement at the depth of ~5 km, (e.g. Jia et al., 2003, Jia et al., 2006, Jia et al., 2010; Jin et al., 2010; Hubbard and Shaw, 2009; Hubbard et al., 2010; Lu et al., 2012, Lu et al., 2014; Li et al., 2013; **Figure 2A**). Deeper deformation is concentrated in the front of the Longmen Shan, but part of shortening may have propagated a little forward, resulting in the formation of blind structures (Wang et al., 2014a). In contrast, wide and gentle folds are identified in the northern segment (north of Anxian) (**Figure 2C**). These structures involve a much deeper structural level (>10 km in depth) and did not produce large structural relief (Jia et al., 2006; Chen et al., 2008; Jia et al., 2010; Jin et al., 2010; Wang et al., 2014b; Chen et al., 2019). Previously, they were considered as concentric folds, but new high-resolution seismic profiles suggested that except the basal décollement, deformation there was decoupled by at least another two décollements, as lots of small-scale folds have been identified solely in the middle structural level (Wang et al., 2014b; Chen et al., 2019; **Figure 2D**). In center segment between the Dujiangyan and Anxian, deformation is also decoupled by the Triassic salt décollement, but in a very low degree as both shallow and deep structures still focus on the front of Longmen Shan (**Figure 1**, **Figure 2B**).

Within the *WSFTB*, several locally or regionally distributed weak rock layers like the Triassic and Cambrian salts and the Silurian shale (**Figure 3**), may have taken advantage to decouple the deformation and form distinct structural styles within different structural levels and along the strike as mentioned above (Cai and Liu, 1997; Jia et al., 2006; Tang et al., 2008; Jin et al., 2010; Lu et al., 2012; Li et al., 2013; Li et al., 2014; Chen et al., 2019; **Figure 2**). Recently, Cui et al. (2020) conducted sandbox experiments and illustrated that the Triassic salt décollement could account for nucleation of the Longquan anticline far into the Sichuan Basin. Using the same method, Fan et al. (2020) found that synchronous participation of the Triassic and

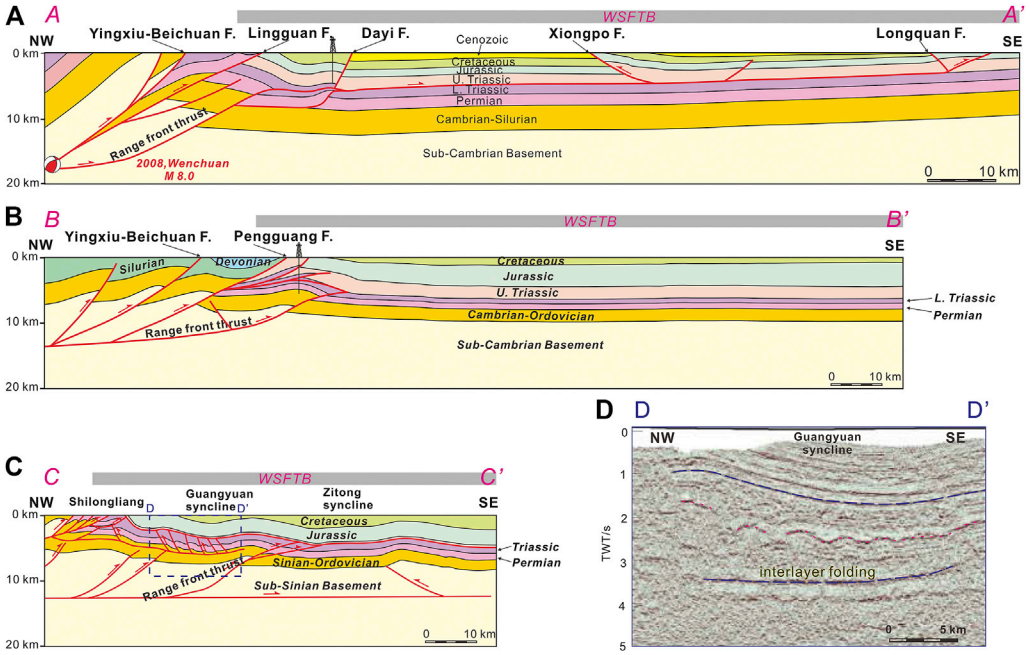

FIGURE 2 | (A and B) Cross sections across the southern and central segment of *WSFTB* (after Li, 2014). **(C)** Typical cross section from the northern segment of *WSFTB*, modified from Li. (2014) and Chen et al. (2019); **(D)** New obtained high-resolution seismic profile across the Guangyuan syncline from Chen et al. (2019), showing folding that confined in the middle structural level. The locations of these four profiles are indicated on **Figure 1**, roughly.

Cambrian décollements provided an essential condition for the formation of blind duplex in the northern *WSFTB*. Their contributions confirmed that the activation of different décollements was the main reason for the presence of along-strike structural diversity. However, there lacks a comprehensive understanding of how contrast structures along the ~500 km-long *WSFTB* were developed. For example, the Triassic salt décollement is evenly distributed within the western Sichuan Basin (Jia et al., 2006; Li, 2014), but it is not clear why the decoupling in its southern segment is much more outstanding. Meanwhile, factors controlling the differential deformation migration within deep structural levels (beneath the Triassic salt) are also poorly investigated.

Weak rock units like salt or shale, as well as the planes between sediments and base of the basin (potential décollements) stand at the forefront in controlling structural style of a fold-and-thrust belt (Davis et al., 1983; Davis and Engelder, 1985; Dahlen, 1990), and have been extensively explored by analogue and numerical modeling methods, (e.g. Cotton and Koyi, 2000; Koyi et al., 2000; Bonini, 2001; Couzens-Schultz et al., 2003; Bonini, 2007; Storti et al., 2007; Graveleau et al., 2012; Ruh et al., 2012; Feng et al., 2015; He et al., 2018; Zhang et al., 2019). These studies suggest that the resultant deformation patterns are sensitive to the rheology, thickness and strength of décollements. They also found the close relationship between along-strike structural variations and lateral changes of the décollements, as proposed for the southern belt of the Tian Shan in China (Borderie et al., 2018), the Salt Range in Pakistan (Cotton and Koyi, 2000; Borderie et al., 2018), the external zone of Gibraltar Arc between the Africa and Europe (María et al., 2003), the northern Apennines in Italy (Massoli et al., 2006) and the Zagros belt in Iran (Koyi et al., 2000; Bahroudi and Koyi, 2003; Ali and Koyi, 2014). These previous studies, however, mainly explored the cases of single or two décollements. Stratigraphy containing more than two décollements like that of the Sichuan Basin is poorly studied (Yan et al., 2016; Huang et al., 2020). Moreover, most of them only focused on the map-view structural and geomorphic changes, conditions beneath shallow décollement (important structural levels in the Sichuan Basin for petroleum resources and seismicity) received much less attention.

In this study, we conducted 2D sandbox experiments with a simplified stratigraphy of the WSFTB. We fixed basal and shallower décollement like that in Cui et al. (2020) and Fan et al. (2020), but a third one was added between them to represent the mid-level, locally distributed décollements such as the Cambrian salt or the Silurian shale (**Figure 3**). This is based on the structural style analysis (**Figure 2**) which leads us to speculate that along-strike variation of this third décollement may have played an important role in shaping current WSFTB. We varied this mid-level décollement (*MD*) both from absence to presence and from frictional to viscous in three experiments (**Figure 4**). Their results are found comparable with the southern, central and northern *WSFTB* respectively, which consequently confirmed our speculation about the formation of the *WSFTB*. Further, they also allow us to assess the role of different *MD*s on deformation propagation in each structural level and the activation of other

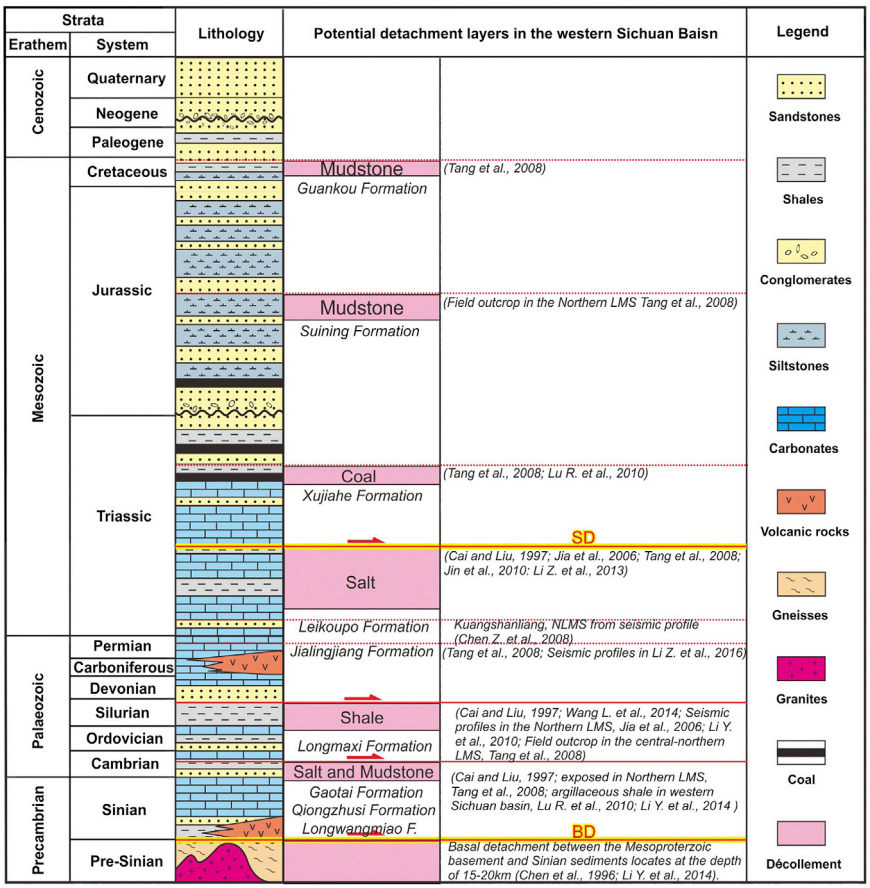

FIGURE 3 | Décollement layers in the *WSFTB* summarized from Chen and Wilson. (1996); Cai and Liu. (1997); Jia et al. (2006); Chen et al. (2008); Tang et al. (2008); Jin et al. (2010); Li et al. (2013); Li et al. (2014); Li et al. (2016).

décollements, which shed new light on the evolution of multiple décollement systems not only the *WSFTB*.

2. GEOLOGICAL SETTING

The Sichuan Basin (western China) covering an area of 2.6 × 10^5 km^2 is a large petroliferous basin that currently bounded by mountain belts all round. As a superimposed basin developed on a Proterozoic cratonic basement, it has experienced several episodes of extension and compression near its boundary, and has accumulated >10 km thick layer-cake stratigraphic architecture during its long evolution history. Two major stages were distinguished corresponding to the stratigraphic architecture changing from late Paleozoic to early Middle Triassic marine sequences to post Middle Triassic wedge-shaped terrestrial strata, (e.g. Li et al., 2003; Meng et al., 2005; Jia et al., 2006; Yan et al., 2011; Yan et al., 2018; Liu et al., 2020). Within this thick sedimentary cover, a large number of incomplete or weak rock units were found activated as décollement layers on outcrops and interpreted seismic profiles, for example the argillaceous siltstone of Cambrian, the black coaly shale of Silurian and the halite-salt of Triassic in marine stratum at the lower-middle structural levels, as well as the shallow-level coal and mudstone of upper Triassic and Jurassic, (e.g. Chen and Wilson, 1996; Cai and Liu, 1997; Chen et al., 2005; Jia et al., 2006; Tang et al., 2008; Jin et al., 2010; Li et al., 2010; Lu et al., 2012; Li et al., 2013; Li et al., 2014; Wang et al., 2014b; Li et al., 2016; Chen et al., 2019; **Figure 3**).

Décollement layers are the major paths for deformation propagation from the basin margins to its interior. Our study area (*WSFTB*) is adjacent to the major tectonic boundary where the Songpan-Ganzi terrane (part of current Tibetan Plateau) thrusts over the Sichuan Basin and the Longmen Shan forms (Zhao et al., 2012; Guo et al., 2013). Structurally, the *WSFTB* is the thin-skinned part of Longmen Shan orogen and displays strong segmentation along its strike, (e.g. Jia et al., 2006; Jin et al., 2010). Taking Dujiangyan and Anxian as the boundaries like the Longmen Shan in the hinterland, (e.g. Li et al., 2010), it can be divided into three segments. The southern-central segments are delineated by the >200 km long Longquan anticline (**Figure 1**) which represents the shallow deformation front of the Longmen Shan orogen (**Figure 2A**). Between this anticline and the foothill of the Longmen Shan, a ~100 km wide Paleogene-Neogene basin with deposits <1000 m thick has developed. Within this restricted basin, several shallow fault-related fold

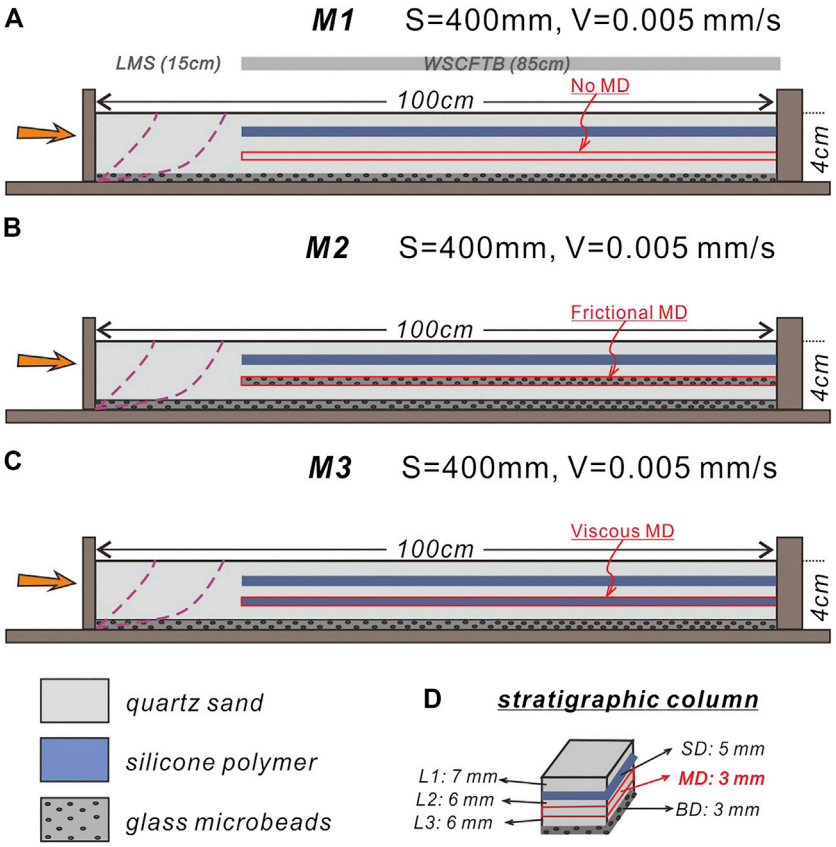

FIGURE 4 | Experimental designs. The layers outlined by red are our investigated mid-level decollements. All the other boundary conditions are identical in the three experiments. SD: shallow décollement; MD: mid-level décollement; BD: basal décollement.

structures like the Dayi and Xiongpo anticlines have emerged or are buried (**Figure 2**), and recent low-temperature thermochronological data suggests that they developed by an in-sequence manner above the Triassic salt décollement, (e.g. Jia et al., 2020). However, it is noted that most of the emerged structures nucleate within the southernmost segment. In the central segment (north of Dujiangyan), only the Longquan anticline show clear geomorphology. While regarding the north segment, there exist few emerged structures as the Longquan anticline has plunged before reaching Anxian (**Figure 1**). Except for the shallow structural variations above the Triassic salt, the subsalt deformation and its relationship with shallow structural level change along the strike as well. The southern segment with the farthest shallow deformation front has a deep deformation front restricted near the foothill of the Longmen Shan (**Figure 2A**). A range front ramp fault there connects the basal décollement beneath the Longmen Shan orogen with shallow décollement in the western Sichuan Basin, forming a crustal scale flat-ramp-flat structural system (Hubbard and Shaw, 2009; Hubbard et al., 2010; Li et al., 2014; Li et al., 2016). In the central segment, a structural wedge has occurred beneath the shallow splay faults (Li et al., 2010; Lu et al., 2016; Lu et al., 2018; **Figure 2B**). Although deformation fronts in both shallow and deep structural levels are close, they are decoupled. As to the northernmost segment, layered deformation controlled by décollements at different depth becomes more pronounced and complex (Wang et al., 2014b; Chen et al., 2019; **Figure 2C**), especially a series of small folds independent of regional structures have developed within the middle structural level interbedded by two décollements (**Figure 2D**).

Most of modern structures adjacent to our study area (especially within the Longmen Shan orogen) display rather linear and continuous geometry (**Figure 1**). However, evidence for along-strike variation in the tectonic evolution has been widely recognized (Jia et al., 2006; Jia et al., 2010; Jin et al., 2010; Yan et al., 2011; Yan et al., 2018), indicating that the existence of contrast stratigraphic architectures. Terrestrial strata in the shallow structural level are associated with formation of the Longmen Shan there and two major orogenic events could be identified (Burchfiel et al., 1995; Jia et al., 2006; Jia et al., 2010). The first one witnessed by wedge-shaped terrestrial clastic rocks took place in Late Triassic to Late Cretaceous times when the Songpan-Ganzi ocean basin closed (Luo and Long, 1992; Liu et al., 1996; Meng et al., 2005; Liu et al., 2012; Liu et al., 2020). It produced flexurally loaded foredeep affecting the whole western margin of the Sichuan Basin (Li et al., 2003; Jia et al., 2006). During this evolution, significant lateral migration and expansion

of the foredeep (from the south to north) occurred, possibly related with clockwise rotation of the Sichuan Basin (Meng et al., 2005). The latest event is related to the India-Asia collision (Burchfiel et al., 1995; Chen and Wilson, 1996) and only very limited Cenozoic sediments were preserved in the southwest conner of the basin. Taking this nonmarine sedimentary rocks in the western Sichuan Basin as a whole, their thickness is relatively small (maximum thickness in foothill of the Longmen Shan, ~5 km). Weak rock units therein only show decupling locally in the mountainous area (Tang et al., 2008). Therefore, their deformation style and the along-strike difference are probably more controlled by behaviors of the Triassic salt and marine strata beneath (**Figure 2**).

With regard to the marine strata in middle-deep structural levels, several intracratonic sags and palaeo-uplifts of different ages were developed beneath the Triassic salt (Liu et al., 2020 and references therein). The sags occurred in the central-northern segments of the western Sichuan Basin, while the uplifts nucleated in the southern-central segments (Figure 14 in Liu et al., 2020). They all orient at high angles to modern Longmen Shan orogen and may have greatly affected stratigraphic architectures, thus contribute to along-strike variation of weak rock distribution. Coincidentally, deformation complexity beneath the Triassic salt also varies, with weak rock units showing different degrees of decoupling along strike of the *WSFTB* (**Figures 2**, **3**). Therefore, we speculate that the potential décollement layers and their along-strike changes (in this marine strata) have played important roles during the deformation. Moreover, considering the Triassic salt extends steadily beneath the western Sichuan Basin, we also suggest that the middle-level décollement may have not only affected the middle-deep structural deformation, but controlled the shallow deformation as well.

3. ANALOGUE MODELING

3.1 Modeling Setup

Our experimental apparatus is a 100 cm-long, 30 cm-wide glass-sided box with a horizontal PVC base. Backstop in the left connects with computer-controlled motor that provides shortening for the models, while the right side is fixed (**Figure 4**).

Analogue of stratum in the Western Sichuan Basin is carefully designed and installed in the sandbox. In all our experiments, one basal frictional décollement (BD) and one shallow viscous décollement (SD) are introduced constantly at the same structural levels, simulating the décollement between sedimentary cover and the basement of Sichuan Basin and the regional distribution of Triassic salt décollement, respectively (**Figure 3**). A third décollement has been inserted between the shallower and basal ones (**Figure 4**). The rheology of this middle-level décollement is the only variable. We alter it from absence (no weak materials added as a middle-level décollement in Exp. M1, **Figure 4A**) to presence (frictional middle-level décollement in Exp. M2 (**Figure 4B**) and viscous middle-level décollement in Exp. M3 (**Figure 4C**). The latter two are representatives of the Silurian shale and Cambrian salt, respectively (**Figure 3**), or other locally distributed décollements at similar structural level.

3.2 Modeling Materials

Like many previous sandbox modeling studies, (e.g. Weijermars et al., 1993; Cotton and Koyi, 2000; Bahroudi and Koyi, 2003; Nilforoushan et al., 2008; Wu et al., 2014; Sun et al., 2016, Sun et al., 2019; Yan et al., 2016; He et al., 2018; Cui et al., 2020; Fan et al., 2020), we use dry quartz sand, glass microbeads and viscous silicone polymer to build rheologically analogous stratum of the Sichuan Basin.

The first two materials deform in a brittle manner and obey the Coulomb failure criterion, thus are suitable representatives for the brittle crustal rock (Colletta et al., 1991; Lohrmann et al., 2003; Panien et al., 2006; Ritter et al., 2016). In our experiments, sieved quartz sand (grain size of 0.2–0.4 mm) serves as principal part of model stratum, simulating competent rock units in the WSFTB. The sand pile has an internal friction of around 0.7, a cohesive strength of ~150 Pa and a bulk density of ~1400 kg/m^3. Layers of glass microbeads are introduced as brittle frictional décollements (normal pressured shale or mudstone, coal layer or the plane between sediments and the basement), because they have a lower frictional strength (approximately 0.4) than dry quartz sand and are able to slip easily due to their spherical shapes (Krantz, 1991; Klinkmüller et al., 2016). The used glass microbeads are cohesiveless and have a mean diameter of 0.3 mm with a density of ~1000 kg/m^3. We choose Newtonian silicone polymer to simulate viscous detachments like overpressured shale, salt and gypsum, (e.g. Borderie et al., 2018; Wang et al., 2019). Because at typical laboratory strain rates, the rheological characteristics of silicone putty are consistent with the salt rock at geological strain rate (Weijermars and Schmeling, 1986; Weijermars et al., 1993; Reber et al., 2020). The density of the silicone putty used here is ~1000 kg/m^3 and the viscosity is about 10^4 Pa.s at room temperature (24°C).

3.3 Scaling

Reasonable models should be properly scaled with nature in geometry, kinematics, and dynamics (Weijermars and Schmeling, 1986). Mechanical properties of used materials and their ratios to the prototype determine the finally length and kinematic scales, (e.g. Ritter et al., 2016). For the brittle deformation, the Smoluchowsky number (S_m, Ramberg, 1981) is a commonly used benchmark, which is defined by the ratio of the gravitational force ($\sigma = \rho g h$) to the frictional force ($\tau = \mu\sigma + C$), where μ and ς are friction coefficient and the cohesion. Dynamic similarity is achieved when this ratio is of the same order in nature and the sandbox. Because the friction coefficient of sand and real brittle rocks is similar (Colletta et al., 1991; Lohrmann et al., 2003), a simplified length ratio $\left(\frac{h_m}{h_n} = \frac{C_m \rho_n}{C_n \rho_m}\right)$ is therefore obtained. Taking mechanical properties listed in **Table 1**, it is calculated to be ~2.5×10^{-6}. As a result, 1 cm in our sandbox represents 4 km in nature.

As for the time-dependence viscous deformation, we use the Ramberg number (R_m, Weijermars and Schmeling, 1986) that represents the ratio of gravitational to viscous forces: $R_m = \frac{\sigma}{\tau} = \frac{\rho g l}{\eta \varepsilon}$. Assuming that simple shear dominates within the viscous layer, τ here can be transferred as $\tau = \eta\varepsilon = \eta\frac{v}{l}$. This gives the velocity ratio as $\frac{v_m}{v_n} = \frac{\rho_m l_m^2 \eta_n}{\rho_n l_n^2 \eta_m}$. Based on materials properties (**Table 1**), GPS velocity of 4 ± 2 mm/yr (Zhang et al., 2004; Gan

TABLE 1 | Material properties and scaling parameters between model and nature.

Quantity	Unit	Nature (n)	Model (m)	Scaling ratio (m/n)
Length/Thickness (h)	m	16000	0.04	~2.5×10^{-6}
Gravity acceleration (g)	m/s^2	9.81	9.81	1
Density (brittle rocks of upper crust, ρ_b)	kg/m^3	2400	1400	0.6
Density (rock salt, ρ_s)	kg/m^3	2200	~1000	0.45
Viscosity (rock salt, η)	Pa·s	10^{19}[a]	10^4	10^{-15}
Friction coefficient (brittle rocks,μ)	–	0.6–0.85[b]	0.7[c]	~1
Cohesion (brittle rocks, C)	Pa	6×10^7[d]	≤200[c]	~3.3×10^{-6}
Coulomb failure occurring above basal detachment				
Stress ($\sigma = \rho g h$)	Pa	3.8×10^8	549	1.5×10^{-6}
Simple shearing within the shallow viscous décollement (~4000 m deep in nature vs. 1 cm deep in model)				
Strain rate (ε)	s^{-1}	9.4×10^{-12}	1.4×10^{-2}	1.5×10^9
Shortening rate ($v = \varepsilon l$)	–	4 ± 2 mm/yr[e,f]	3.75×10^{-4} mm/s	3750

[a]*Van keken et al. (1993)*
[b]*Byerlee. (1978)*
[c]*Wu et al. (2014)*
[d]*Weijermars et al. (1993)*
[e]*Zhang et al. (2004)*
[f]*Gan et al. (2007)*

et al., 2007) and the same length scale as the brittle deformation, we calculate the experimental shortening rate as ~10^{-4} mm/s. However, this value is too small to be carried out in the experimental platform. We therefore apply a shortening rate of 0.005 mm/s instead to all the present experiments.

3.4 Construction

After cleaning the sandbox with alcohol solution and drying, we first deposit a 3 mm-thick glass microbeads layer in the sandbox as the basal décollement (BD). Then, layers of quartz sand are sieved to build competent rock units from a constant height of 40 cm (to ensure the homogeneity of resultant sand piles). The used color sand has the same mechanical property as the white sand, they just act as passive markers to identify the ongoing deformation. When introducing the shallower décollement (SD, 5 mm thick), a 15 cm-long gap is left between the mobile backstop and pinch-out of the décollement. This design allows the formation of a thrust wedge like the Longmen Shan orogen before deformation reaches the basin area (Sun et al., 2016; Cui et al., 2020; Fan et al., 2020). Notably, the *MD*s in Exp. M2 and Exp. M3 cover the same region as the *SD* (**Figures 4B,C**), with a fixed thickness of 3 mm (**Figure 4D**). The total thickness in all experiments is identical, at 4 cm. According to the length scale ratio, it corresponds to 16 km in nature.

We stress that all décollements in the experiments are chosen as 3 mm-thick artificially (that is 1200 m in nature, thicker than their prototypes), as thinner layers are difficult to deposit. The depth of corresponding décollement is also forced at the same level for all the three experiments for simplification.

4. RESULTS

In this section, we describe the cross-sectional evolution of our experiments to show how differential deformation is induced by the investigated *MD*s.

4.1 Experiment M1: No Middle-Level Décollement

There were two décollements in this experiment, including the basal one covering the whole sandbox and the shallower one distributed only in the foreland (**Figure 4A**), while no MD was considered. Experimental shortening induced deformation ahead of the moving backstop immediately. During the first 78 mm of shortening, two in-sequence thrusts (F1 and F2) nucleated and emerged (**Figures 5A–C**), as there was no shallow décollement within the involved sand pile yet. They both dipped at ~35° in their initial stage. During successive shortening, the two faults progressively stacked against the backstop. At 120 mm of regional shortening, deformation was propagated forward and began to affect the foreland area where shallow viscous décollement was situated (**Figure 5D**). In response, two new structures, namely the deep thrust F3 and the shallow fold S1 formed. They were separated by the *SD*. The blind thrust F3 displayed an gentle initial dip angle at ~20°. It merged into the *SD* and continued taking up the experimental shortening and transferred displacement to the shallower level. During this stage, deformation propagated only in the shallow level with the nucleation of detachment folds S2 and S3 (**Figures 5D–F**). The space between S2 and S3 was ~10 cm, smaller than that of F3, ~16 cm. Once the shortening reached 258 mm, another blind thrust F4 was developed in the deep structural level (**Figure 5G**). The deep deformation front stepped out at a distance of ~24 cm. After that, F4 and its conjugated fault F5 nucleated and became the major structure that accommodated the regional shortening (**Figures 5G–J**), similar to the role of F3 during previous stages (**Figures 5D–F**). While in the shallow level, a total of four detachment folds (S4–S7) occurred, representing another period of rapid shallower deformation propagation. This experiment finally ended up with a total shortening of 400 mm (**Figure 5J**). At the latest stage, another deep thrust F6 was generated ~30 cm away from F5, following the appearance of a low-amplitude fold geometry beneath S5 and S6.

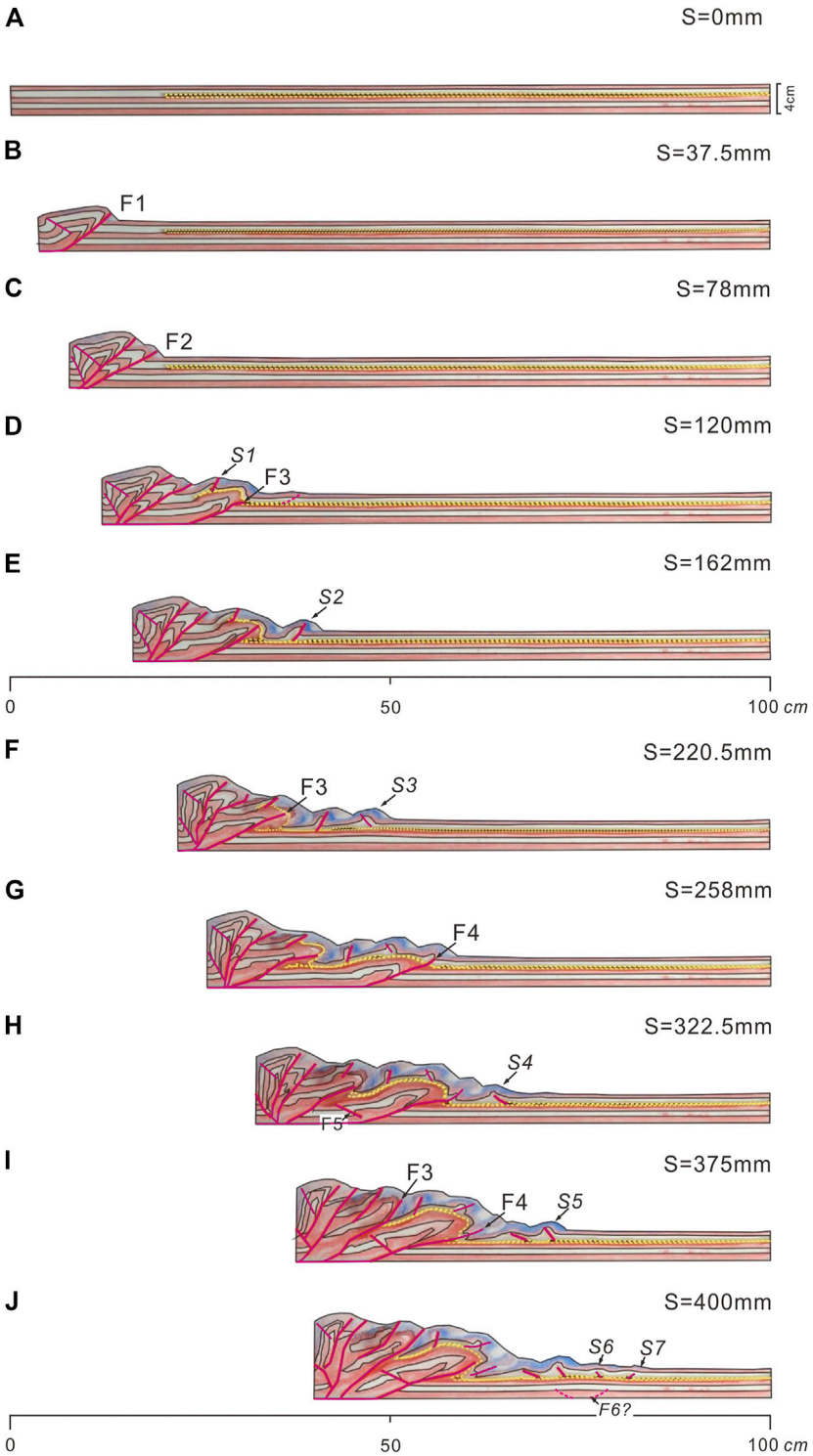

FIGURE 5 | Evolutionary stages of Exp. M1 that contains no MD. The yellow dash line outlines the viscous SD. On the base of the model, a frictional *BD* was also added. Uppercase letters S and F are used to indicate Folds involving the shallow structural level (above the SD) only and thrusts nucleated from the basal décollement. **(A–C)** early stages before the SD was affected by shortening; Experimental shortening produced a thrust wedge against the mobile backstop (not shown here). **(D–J)** Deformation started its propagation within the shallow and deep structural levels (separated by SD), respectively. A fast, in-sequence development of shallower folds occurred synchronous with deep faulting. Shortening in deep was localized in fewer faults in comparison to the shallow, resulting in a delay in the migration of the deep deformation front toward the foreland.

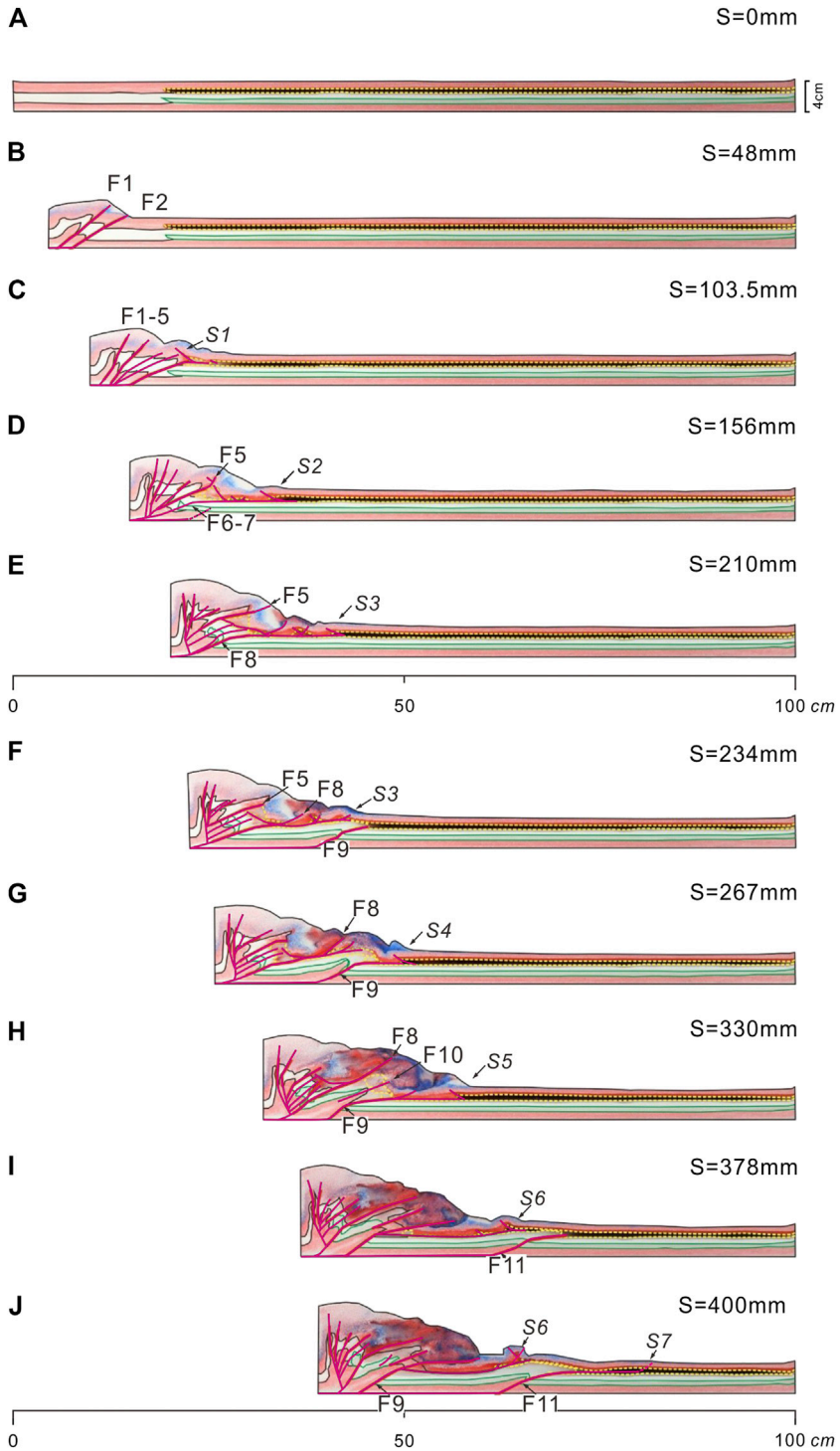

FIGURE 6 | Evolutionary stages of Exp. M2 that has a frictional *MD* (outlined by green line). The yellow dash line outlines the viscous SD. A frictional BD was also added on the base of the model. Uppercase letters S and F are used to represent folds involving the shallow structural level (above the SD) only and thrusts nucleated from the basal décollement. **(A–B)** initial stacking of small thrust slices in the right; **(C–E)** deformation started to affect the shallow structural level (above the SD). Synchronously, small thrusts F6–7 nucleated beneath the SD; **(F–J)** Asynchronous deformation propagation in the shallow and deeper structural levels. The deeper faults in these stages showed much large spaces than the former stages.

The fault space in deep structural level increased with their sequence. In contrast, the shallow ones remained similar, in the range of 6–10 cm. Vergence of these shallow folds were random, consistent with Davis and Engelder. (1985)'s prediction about fold-and-thrust belts over salt décollement.

Overall, this experimental model run without *MD* displayed fast, shallow propagation of deformation toward the foreland, and episodic step of deep deformation front in the deep.

4.2 Experiment M2: Frictional Middle-Level Décollement

In contrast with Exp. M1 that had no MD, a middle-level layer of glass microbeads was added in this experiment (**Figure 4B**). This was simulating the potential MD consisting of shales or coal bed in the center *WSFTB* (**Figure 3**). The initial deformation still took place by in-sequence nucleation of closely space (1–2 cm) thrusts against the moving backstop (**Figures 6A–C**), but four faults (F1–F4) had formed before *SD* in the foreland was involved, which were double of those in Exp. M1 at the same stage (**Figure 5C**). They showed an average dip angle of ~33°, and were counterclockwise rotated in the following shortening. When the fifth thrust F5 showed up beneath the SD, a shallower backthrust-dominated fold S1 also emerged. They together with the imbricate fan containing F1–F4 made up a passive roof duplex (**Figure 6C**). Interestingly, the dip angle of F5 was just ~20°.

As experimental shortening continued, both the deep and shallower deformation fronts propagated toward the foreland (**Figures 6C–E**). But the rate of propagation of the shallower system was faster than the deeper system. Moreover, we noted that the propagation rate of the deep deformation was also lower than its counterpart in Exp. M1 after the deformation reached the multiple layered pile, as it progressed in the form of small blind thrusts F6–F8 (**Figure 6E**). When the shortening amounted to 234 mm, the first long (~18 cm) thrust sheet F9 came out beneath the SD, which helped the deep deformation front catch up with the shallower one (**Figure 6F**). Notably, during the same period, strong vertical stacking of thrust sheets was in progress near the moving backstop. With continuous shortening, thrust F8 in the hinterland then truncated the roof sequence of the duplex and emerged in the high-relief slope (**Figure 6G**). This fault along with another out-of-sequence fault F10 and F9 in the foreland acted as major shortening absorbers and caused structural thickening nearby. During the same period, part of shortening was transferred to the shallow level, promoting the occurrence of S5 and S6 there (**Figures 6H,I**).

When shortening came to 378 mm, another blind thrust F11 nucleated ~24 cm away from F9, with the previous shallower detachment fold S6 located in its backlimb (**Figure 6I**). From then till the end of 400 mm shortening, the whole foreland shallower level (above the SD) was progressively detached from the deeper on the shallow décollement. This resulted in rapid flow of the viscous material of SD into a weakly folding structure S6 in the foreland (**Figures 6H–J**). The space between shallow folds was random, due to the distortion from formation of deeper structures.

4.3 Experiment M3: Viscous Middle-Level Décollement

A viscous MD analogue to viscous décollement like salt or overpressured shale, was introduced in this experiment (**Figure 4C**), at the same depth as the frictional décollement in Exp. M2 (**Figure 4B**). While the initial deformation was more similar to Exp. M1 that had no MD (**Figures 6A–C**), with in-sequence formation of two thrusts F1 and F2 during the first 45 mm of shortening (**Figures 7A,B**). They both dipped at ~33°. Once the shortening reached 75 mm, deformation came to the foreland multiple décollement system (**Figure 7C**). The third thrust F3 was developed and a small shallower fold S1 also nucleated from the SD. The dip angle of F3 was also ~20°, similar to its counterparts F3 in Exp. M1 and F5 in Exp. M2. As experimental shortening continued, an out-of-sequence fault F4 emerged in the hanging wall of F3 (**Figure 7D**).

When the experimental shortening reached 168 mm, most of the intermediate level (between the SD and MD) was affected by long-wave (~8 cm) folding (**Figure 7E**). The amplitude of these folds decreased from ~2 cm (beneath S4) toward the foreland. Regarding the right fixed backstop, folding of the sand layer was already too small to be identified. At the same time, a wedge-front syncline bounded by S1 and newly formed S2 developed in the shallow level, synchronously with nucleation of blind F5 near the pinch out of MD. With continued shortening, the amplitude of folds detaching on the intermediate level increased (**Figures 7F–I**), and the fold geometry also evolved from symmetry to asymmetry with the forelimb overturned progressively. At the shortening of 211.5 mm, 307.5 mm and 358.5 mm, three thrusts f1, f2 and f3 hve nucleated in-sequence and truncated forelimbs of the associated intermediate folds respectively. Synchronous with folding and contraction at the middle structural level, the shallow level was also folded. Uplift caused by folding beneath the SD had driven flow of the viscous materials and produced another five shallower structures, S3–S8 (**Figures 7E–J**). However, they were generated under the influence of deeper deformation, which did not obey an in-sequence manner. In contrast to both shallow and intermediate structural levels, deformation in the deep level highly focused on the hinterland. Five closely spaced thrusts F6–F10 had stacked there, forming blind imbricates that merged into the MD. By the end of 400 mm experimental shortening, no long thrust sheets like F4 in Exp. M1 (**Figure 5G**) and F9 in Exp. M2 (**Figure 6I**) have ever developed in this experiment.

5. DISCUSSION

5.1 Effect of MDs on Lateral Deformation Propagation

The three experiments we described illustrate that the response of foreland multiple layered system (like the western Sichuan Basin) to regional shortening relies heavily on the MDs. The presence or absence of MD will lead to significant difference in lateral propagation of deformation at each structural level, thus control the resultant structural styles. We measured the width of the deforming zone at the shallow/intermediated/deep

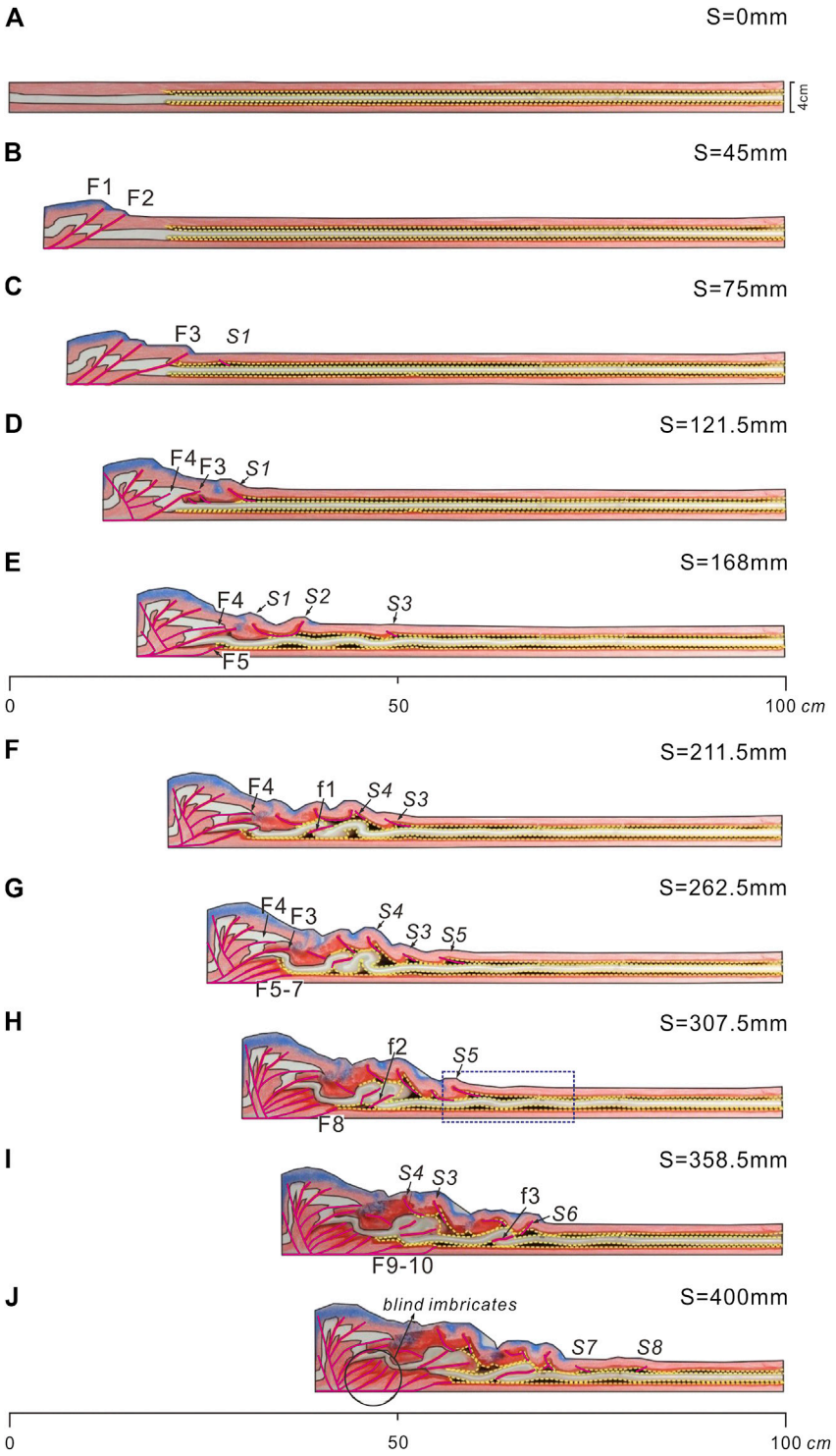

FIGURE 7 | Evolutionary stages of Exp. M3 that includes a viscous MD (marked by yellow dash line, the same as the SD above). Uppercase letters S and F indicate Folds involving the shallow structural level (above the SD) only and thrusts nucleated from the basal décollement. Lowercase letter f is used to label faults limited in the middle level (between SD and MD). **(A–C)** Thrust stacking stages before SD in the foreland were involved by shortening; **(D–J)** Layered deformation within the foreland multiple décollements system. Notably, the mid-level folding affected most of the foreland area very quickly, from **(D)** to **(E)** with ~45 mm of shortening. This fast deformation propagation toward the foreland controlled the styles of successive deformation in both the shallow and deep levels. See the text for details.

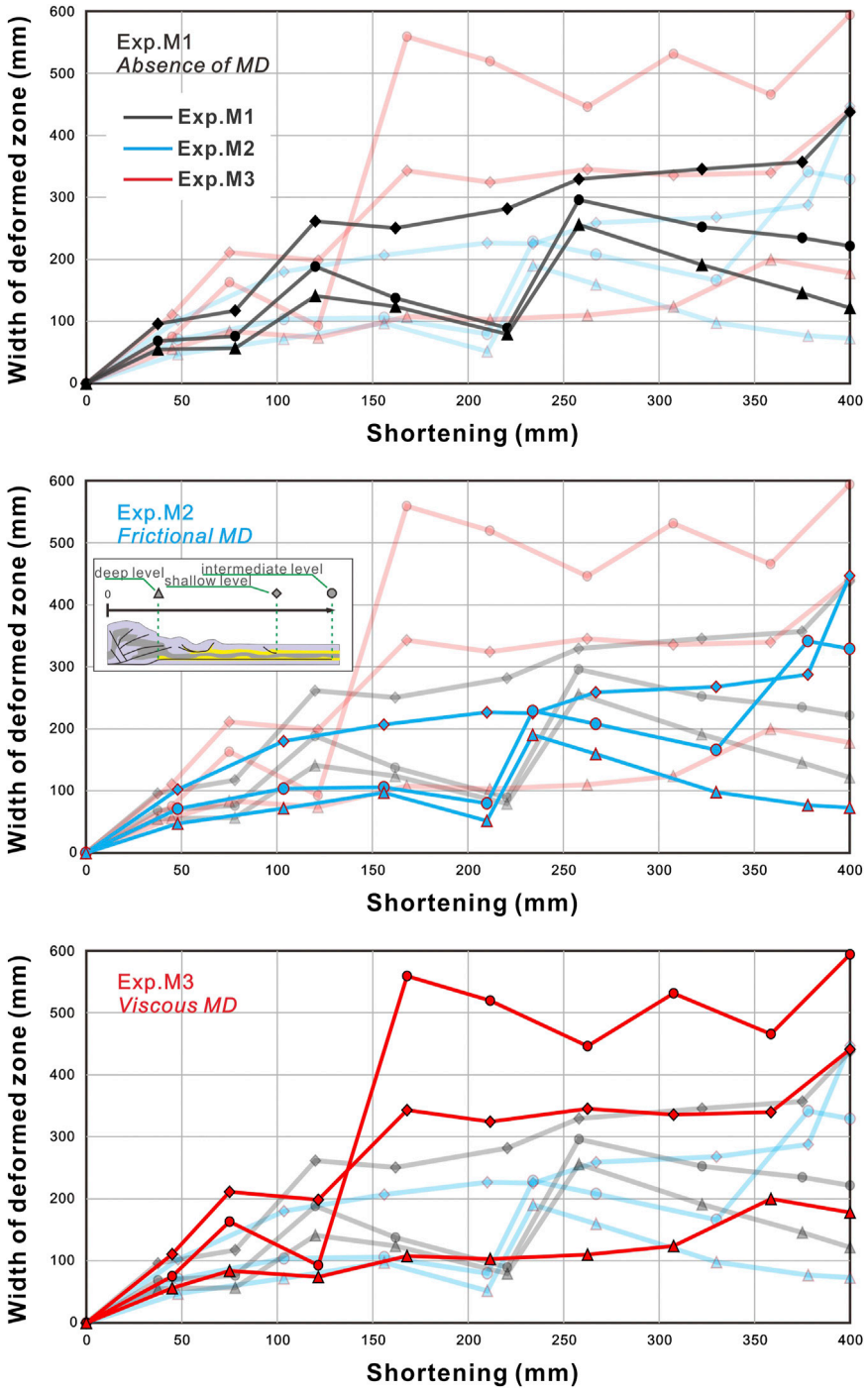

FIGURE 8 | Width curves of deforming zones in the three sandbox experiments. Each experiment has three curves to illustrate the difference in foreland-ward deformation propagation at different structural levels separated by the SD and MD. Approximating curves in one model indicate coupling between them. Otherwise, decouple occurred.

structural levels (separated by the SD and MD, or situated at the corresponding depth when MD was absent in Exp. M1), and obtained three lateral growth curves for each experiment at the same levels (**Figure 8**). Approximating curves in one experiment suggested that deformation within the corresponding structural levels were coupled. While a greater difference on them indicated a stronger decoupling effect. They thus help to quantitatively constrain the differences in modeled deformation.

In Exp. M1, there is no MD in the foreland multiple layered system (**Figure 5A**). The intermediate-deep structural levels are

therefore coupled during the whole evolution. Longer, blind thrust sheets with the boundary faults cutting both levels occurred (**Figures 5D–J**), resulting in episodic propagation of deformation toward the foreland (black sawtooth-type growth curves with circles and triangles in **Figure 8**). The small difference between lateral growth curves of the intermediate-deep levels is a result of the dip geometry of the deformation front (fore-thrusts). As the shallower structural level above the SD only involved a thin layer (**Figures 4**, **5**), its deformation front stepped toward the foreland rapidly, but with a limited step width each time. Consequently, the growth curve (marked by rhombus) is relatively smooth, in contrast to the intermediate-deep levels.

A brittle frictional MD has been introduced in our Exp. M2 (**Figure 6A**). However, we note that during most of stages (before 330 mm of shortening), the intermediate-deep levels did not experience effective decoupling. The growth curves of them (light blue lines with circles and triangles in **Figure 8**) were comparable with their counterparts in Exp. M1 which lacked an MD. Only in the latest stage (after 330 mm of shortening), a differentiation between curves of intermediated and deep levels occurred, which reflected the initiation of slip or called detachment along the brittle *MD*. Wang et al. (2013c) proposed that a similar interbedded frictional décollement can only be activated when enough vertical loading (syn-tectonic sedimentation in their sandbox experiments) was added. In our experiment M2, a similar process took place with the increased topographic relief, playing the same role as that of syn-tectonic sedimentation in Wang et al. (2013c).

Notably, all growth curves from the Exp. M2 (at each depth, including the shallow level) were similar to, but located below their counterparts in the Exp. M1 (black vs. light blue lines in **Figure 8**). As predicted by the critical taper theory, a thrust wedge composed of weaker materials would have a larger critically tapered angle under which forelandward deformation propagation can be motivated, (e.g. Davis et al., 1983; Dahlen, 1990). The introduction of a frictional MD in Exp. M2 reduced the strength of foreland multiple layered system. Thus, more structural relief (additional stacking of small slice, F6–F7 in **Figures 6C–E**) than Exp. M1 was required to achieve the larger taper. This has resulted in the lower rates of lateral growth we observed.

In our third experiment M3, a viscous MD was added (**Figure 7A**). This led to an extremely weak multi-décollement foreland basin system that effectively decoupled along the SD and MD. The deformation propagation toward the foreland at its shallow (red line with rhombuses **Figure 8**) approximated to that in Exp. M1 and Exp. M2. However, the viscous décollements above and below the intermediate layer were too weak, their resistance to outward deformation propagation was therefore quite small. Thus, after the arrival of experimental compression, the deformation affected most of this intermediated layer rapidly by long-wave gentle folding (**Figures 7E–J**). This gave rise to a sudden forelandward shift in deformation at 168 mm of shortening, characterized by a steep ramp on the growth curve (red line with circles **Figure 8**). After that, the intermediated deforming zone became significantly wider than both the shallow and deep levels, indicating its leading role in deformation of the distal foreland. With regard to the deep structural level, formation of closely spaced thrusts (**Figure 7**) exhibited a smooth growth curve (red line with triangles **Figure 8**). We propose that earlier deformation within its overlying levels increased the loading on it and suppressed its further forelandward deformation migration.

5.2 Comparison With the *WSFTB*

There is no doubt that the presence of décollements controlled the first-order style of the *WSFTB*. Their role in shaping fold-and-thrust belt ahead of the Longmen Shan has been tested by both physical and numerical modeling (Zhang et al., 2019; Cui et al., 2020; Fan et al., 2020), as well as by analytical solution (Hubbard et al., 2010; Zhang et al., 2018). One remarkable phenomenon associated with the décollements is the nucleation of Longquan anticline that extends far into the basin (**Figure 1**). Using sandbox modeling, Cui et al. (2020) showed that weakness of the shallow salt décollement was the dominant factor for the observed fast and further deformation propagation as indicated by the Longquan anticline. However, a problem emerged here about the contrast structural style in the northern segment where the Triassic salt layer exist as well (**Figure 2A** vs. **Figure 2C**). Why does this segment display different deformation style?

The *WSFTB* was developed based upon a multiple décollement system (**Figures 2**, **3**). Through the sandbox experiments in this study, we have illustrated that the mid-level décollement played an important role in determining the deformation mode of a thrust and fold belt. Furthermore, in the *WSFTB*, except for two regionally distributed décollements (the basal one at the bottom of the basin and the shallow one in the Triassic evaporite rocks), several local décollements have also participated in the deformation as identified from both field outcrops and seismic profiles, (e.g. Cai and Liu, 1997; Jia et al., 2006; Tang et al., 2008; Jia et al., 2010; Jin et al., 2010; Li et al., 2010; Lu et al., 2012; Wang et al., 2014b; Lu et al., 2016; Lu et al., 2018; Chen et al., 2019; Wang et al., 2020, summarized in **Figure 3**). Among them, the Silurian shale from the central-northern *WSFTB* and the Cambrian salt/mudstone in the northern segment are two representatives in a middle structural level similar to our investigated *MD*s.

Based on the comparison between our experiments and the typical cross sections, we infer that lateral change in the *MD*s is the main reason for the observed structural variations along the strike of WSFTB (**Figure 9**). As shown by Exp. M1, experimental shortening would be transferred directly through ramp structures that connect the basal and shallow décollements if there was no MD (**Figure 5**). A pronounced shallow folding belt would then form ahead of the ramp before the occurrence of outward-step deformation in the deep level (nucleation of another deep ramp structure) (**Figures 5F,J**). Such a contrast mode of deformation localization in the vertical direction is also a characteristic of the southern *WSFTB* (**Figure 2A**). Meanwhile the shallow folds like S5–S7 in Exp. M1 (**Figure 5J**) are comparable to the Dayi, Xiongpo and Longquan structures that make up the southern *WSFTB* as well. Therefore, except for the Triassic salt décollement and the basal décollements, there may exist no other active regional detachment beneath the southern *WSFTB* (**Figure 9**). This speculation seems to be supported by the discovery that the

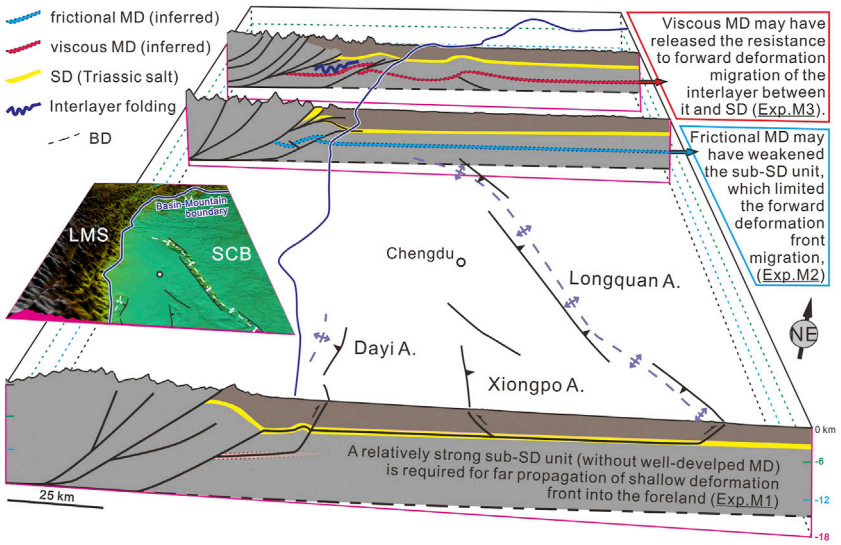

FIGURE 9 | 3D diagram showing how different MDs contribute to structural diversity along the strike of WSFTB. The absence of MD in the south, presence of brittle shale MD in central *WSFTB* and viscous salt MD in the northmost can explain the observed first-order structural differences. Notably, the possible variations of décollements thickness and their depth have not been constrained here.

southern *WSFTB* was dominated by a palaeo-uplift context before the Triassic, (e.g., Wei et al., 2008; Liu et al., 2020).

As to the central-northern *WSFTB*, the deep and shallow deformation fronts are weakly decupled and situated roughly at the same location, both are near the foothill of the Longmen Shan (**Figure 2B**). This is coherent with some scenarios presented in our Exp. M2 that contains a frictional MD (**Figures 6F–H**). Some studies based on field outcrop found local detachment along the Longmaxi formation Shale, (e.g. Tang et al., 2008). As shown by Exp. M2, such limited detachment occurred within the frictional décollement layer when its overriding topography is enough (**Figure 8**). Although decoupling effect of the frictional MD is rather weak, the weakness introduced by it has weakened the bulk strength of the associated structural levels. The weakened horizontal rock units would not sustain too large stress and propagate deformation too far (**Figure 6**). Thus, more deformation (in the form of thrust stacking) had been localized near the hinterland part of the multiple décollement system, which restricted the shortening being transferred to the shallow décollement and in turn reduced the ability of outward deformation migration. Consequently, the Silurian shale here should control structural pattern in the central-northern *WSFTB* by weakening the rock units beneath the Triassic salt instead of being activated directly (**Figure 9**).

In the case of northernmost *WSFTB*, long-wave, low-amplitude folds occur and dominate the subsurface level (**Figure 2C**). They were previously considered as concentric folds. However, new higher-resolution seismic profiles revealed strongly decoupling signs as numerous small folding traces were found confined only within the mid-level unit, (e.g. Wang et al., 2014b; Chen et al., 2019; **Figure 2D**). Such a special structural feature is now well reproduced in our Exp. M3, which has taken a viscous MD into account (for example the area marked by blue rectangle in **Figure 7H**). During this experiment, the structural level interbedded between the SD and MD experienced a totally different deformation style with related to its above and below levels. When compression started to affect the foreland multiple layered system, deformation propagation first took place within this level through buckling (or low-amplitude folding) that involved the whole foreland area rapidly (**Figures 7D,E**). With the increase of experimental shortening, the folds near the hinterland amplified progressively, their forelimbs were overturned and finally truncated by late-formed forethrusts (**Figures 7E–J**). While deformation in both shallow and deep levels were lagging seriously. They (especially the deep structures) would probably overprint and complicate the deformation styles in the mid-level during later evolutionary stages, as observed in the northern *WSFTB* (**Figures 2C,D**, **Figure 9**).

5.3 Implications for Seismicity and Petroleum in the *WSFTB*

The structural similarities between our experiments and the *WSFTB* are helpful to understand the distribution of regional seismicity. In the south-central segments of this belt, the shallow deforming belt extends to the Longquan anticline, involving several other anticlines such as the Dayi and Xiongpo (**Figure 1**, **Figures 2A,B**). All these structures are active, undergoing shortening at a rate of 0.2–0.4 mm/y (Li et al., 2019c). They may have borne earthquakes like the 1976 M_s5.5 Renshou event in the Longquan anticline (Wang and Lin, 2017). In the deep (beneath the Triassic salt), however, the deformation front should still locate near the mountain-basin boundary where the 2008 M_w7.8 Wenchuan earthquake and 2013 M_w6.6 Lushan earthquake occurred. The strength of sub-salt units maybe one important factor contributing to such mode of deformation localization. As shown in our modeling, both the flat-ramp-flat

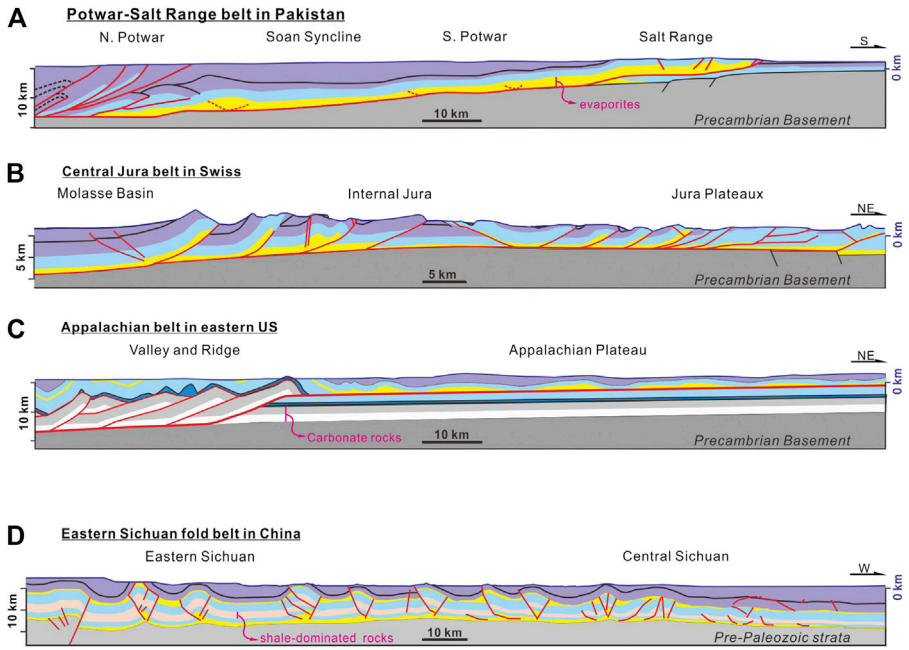

FIGURE 10 | Typical cross sections of **(A)** The Patowar-Salt Rangle FTB in Pakistan (after Jaumé and Lillie, 1988); **(B)** The central Jura belt in Swiss (Affolter and Gratier, 2004); **(C)** The central Appalachian FTB in Pennsylvania, eastern United States (Sak et al., 2012); **(D)** The eastern Sichuan fold belt in China (Gu et al., 2021); Yellow color indicates the involved salt (evaporites) décollements. Other colors are used to show deformation only, not represent specail strata unless being labbed.

system in the south segment (Hubbard et al., 2010; Li et al., 2017; **Figure 2A**) and structural wedge in the central segment (Li et al., 2014; Lu et al., 2017; **Figure 2B**) are indications for lack of regional weak units (like salt rock) in the deep.

With regard to the northmost segment of *WSFTB*, the deformation has been partitioned into shallow, middle and deep levels that were separated by two viscous décollements (Wang et al., 2014b; Chen et al., 2019; **Figures 2C,D**). According to our modeling, the middle-level folding and thrusting should play a key role when the multiple layered foreland system is affected (**Figures 7D,E**). The deformation within the middle level accumulates, uplifts the detached shallow level passively, and exerts more and more loading toward the deep (**Figures 7D–J**). This suppresses forward deformation propagation in the deep and would concentrate shortening within the blind imbricates (**Figure 7J**), which largely account for the 2017 M_s5.4 Qiangchuan earthquake in the northern WSFTB occurring at a depth of ~13 km (Li et al., 2019b).

On the other hand, the northern *WSFTB* has received great attention due to giant gas discovery in the middle-structural-level, upper Paleozoic carbonate rocks, (e.g. Yang et al., 2018; Liang et al., 2019). Through our modeling, we infer that this reservoir stratum may have produced duplex near the mountain front (**Figure 7**). Therefore, apart from "lateral" exploration, the prospect for deeper expedition is also appreciable.

5.4 Implications for Other Fold-And-Thrust Belts (*FTB*s)

Our experiments have produced structural styles resembling with the *WSFTB*, but some features are also comparable with those of several other natural *FTB*s. Taking Exp. M1 as an example, its shallow level deformation is characterized by decupling along the viscous SD. A foreland deforming belt that is much wider than the deeper level one formed (**Figures 5**, **8**). This is comparable with several famous thin-skinned *FTB*s that involve dozens or hundreds of kilometers wide deforming zone over an undeformed basement, for instance the Potwar-Salt Range belt in Pakistan (Jaumé and Lillie, 1988; Ghani et al., 2018; **Figure 10A**), the Jura foreland belt in Swiss (Sommaruga, 1999; Affolter and Gratier, 2004; **Figure 10B**) and the Appalachian Plateau belt in NE United States (Sak et al., 2012; Mount, 2014; **Figure 10C**). There is no doubt that the presence of weak salt décollement has defined a small critical taper angle (≤1°) for these deformed belts (Davis et al., 1983; Davis and Engelder, 1985), which results in fast forward deformation migration. However, except for the surface processes (sedimentation and erosion) and other common factors that can affect deformation migration (see Graveleau et al. (2012) for a review), another important issue should be carefully considered. All these belts are in front part of an orogeny where sedimentary cover is just several kilometers thick. In general, there is only one activated décollement that locates on top of the basement (**Figures 10A,B**) or carbonate rocks (**Figure 10C**), with relatively higher strength compared with shallow clastic rocks. Formation of such remarkable thin-skinned deforming belts seem to require that the sub-salt unit is relatively strong, with limited regional weak strata (potential MD). Our modeling does support this, for if there is either frictional MD (Exp.M2, **Figure 6**) or viscous MD (Exp.M3, **Figure 7**), the foreland shallow deforming zone would more or less reduce compared with the situation when MD is absent (Exp.M1, **Figures 5**, **9**).

The difference in deformation associated with Exp. M1 (no MD) and Exp. M2 (frictional MD) lies in the strength of imposed MD and their spatial distribution (thickness, depth etc.). In natural cases, they may be hard to distinguish. While Exp. M3 can be treated as the end-member case in which the viscous MD has the strongest influence on the resultant structural style. In this experiment, the middle level was interbedded by double viscous décollements and has experienced faster deformation propagation than the shallow and deep ones (**Figure 7**). This exhibits a phenomenon that is also well documented in the eastern Sichuan fold belt where deformation is mainly focused in the middle structural levels with clear intensity decrease from the east Sichuan to its center (**Figure 10D**).

6. CONCLUSION

Motivated by contrast structural styles in the middle structural level of the WSFTB (**Figure 2**), we have conducted sandbox experiments varying the mid-level décollement but fixing basal and shallow décollements to test how the difference in mid-level décollement controls the resultant structural styles of a multiple layered foreland system. Our experiments have produced comparable structural styles with those in the *WSFTB*, indicating that mid-level décollements are major factor controlling the observed along-strike segmentation.

1) Effective decoupling between the shallow and deep structural levels and the pronounced shallow folding belt in the southern *WSFTB* require a rather uniform unit beneath the Triassic salt decollement (no regionally distributed mid-level décollement).
2) Frictional mid-level décollement (the Silurian shale) in central-northern *WSFTB* has weakened the bulk strength of deep structural levels, which limits the deformation fronts of both shallow and deep structural levels in the mountain front.
3) In the north *WSFTB*, fast forelandward deformation propagation in the middle structural level (interbedded between two viscous décollements) controls the deformation above and below. Mountain front duplex within the middle level has good prospects for gas exploration, as regional reservoir stratum involved.
4) In addition to a salt décollement, the pronounced thin-skinned deforming zone of Jura belt in Swiss, the Appalachian belt in NE United States and the Potwar-Salt Range belt in Pakistan also benefit from a relatively strong subsalt unit (without regional weak rocks, like salt).
5) Deformation front in shallow structural level is not always located further forward than the deeper one. Double viscous décollements can give birth to a fast-growing middle-level deforming zone like the eastern Sichuan fold belt, China.

Our experimental results also provide interesting insights for several other fold-and-thrust belt:

DATA AVAILABILITY STATEMENT

The original contributions presented in the study are included in the article/Supplementary Material, further inquiries can be directed to the corresponding author.

AUTHOR CONTRIBUTIONS

CS: Conceptualization, Methodology, Investigation, Writing—original draft, Project administration, acquisition, Supervision, Resources. ZL: Conceptualization, Writing—review and editing, Project administration, Funding acquisition, Resources. SW: Conceptualization, Methodology, Writing—review and editing, Supervision. ZH: Conceptualization, Methodology, Writing—review and editing, SZ and PW : Methodology, Investigation, Visualization.

FUNDING

This work was jointly supported by the National Natural Science Foundation of China (41902201, 41590861, 41772209), the Second Tibetan Plateau Scientific Expedition and Research Program (STEP)(2019QZKK0901) and Guangdong Province Introduced Innovative R and D Team of Geological Processes and Natural Disasters around the South China Sea (2016ZT06N331).

ACKNOWLEDGMENTS

We would like to express our gratitude to two reviewers for their helpful comments, which significantly improved the manuscript.

REFERENCES

Affolter, T., and Gratier, J. P. (2004). Map view retrodeformation of an arcuate fold-and-thrust belt: the Jura case. *J. Geophys. Res.* 109, B03404. doi:10.1029/2002JB002270

Ali, F., and Koyi, H. (2014). Effect of lateral thickness variation of an intermediate décollement on the propagation of deformation front in the Lurestan and Izeh zones of the Zagros fold-thrust belt, insights from analogue modeling. *J. Struct. Geol.* 65, 17–32. doi:10.1016/j.jsg.2014.03.004

Bahroudi, A., and Koyi, H. (2003). Effect of spatial distribution of Hormuz salt on deformation style in the Zagros fold and thrust belt: an analogue modelling approach. *J. Geol. Soc.* 160 (5), 719–733. doi:10.1144/0016-764902-135

Bonini, M. (2001). Passive roof thrusting and forelandward fold propagation in scaled brittle-ductile physical models of thrust wedges. *J. Geophys. Res.* 106 (B2), 2291–2311. doi:10.1029/2000JB900310

Bonini, M. (2007). Deformation patterns and structural vergence in brittle-ductile thrust wedges: an additional analogue modelling perspective. *J. Struct. Geol.* 29 (1), 141–158. doi:10.1016/j.jsg.2006.06.012

Borderie, S., Graveleau, F., Witt, C., and Vendeville, B. C. (2018). Impact of an interbedded viscous décollement on the structural and kinematic coupling in fold-and-thrust belts: insights from analogue modeling. *Tectonophysics* 722, 118–137. doi:10.1016/j.tecto.2017.10.019

Burchfiel, B. C., Zhiliang, C., Yupinc, L., and Royden, L. H. (1995). Tectonics of the Longmen Shan and adjacent regions, central China. *Int. Geol. Rev.* 37 (8), 661–735. doi:10.1080/00206819509465424

Byerlee, J. (1978). Friction of rocks. *Pure Appl. Geophys.* 116, 615–626. doi:10.1007/BF00876528

Cai, L. G., and Liu, H. P. (1997). Structural styles and characteristics of fold-thrust belts in Sichuan foreland Basin. *J. Pet. Explor. Prod. Technol.* 19 (2), 115–120. doi:10.11781/sysydz199702115

Chen, S. F., and Wilson, C. J. L. (1996). Emplacement of the longmen Shan thrust-nappe belt along the eastern margin of the Tibetan plateau. *J. Struct. Geol.* 18, 413–430. doi:10.1016/0191-8141(95)00096-8

Chen, Z. X., Jia, D., Zhang, Q., Wei, G. Q., Benliang, L., Wei, D. T., et al. (2005). Balanced cross-section analysis of the fold-thrust belt of the Longmen Mountains. *Acta Geol. Gansu.* 79, 38–45. (in Chinese with English abstract). doi:10.3321/j.issn:0001-5717.2005.01.005

Chen, Z., Jia, D., Wei, G., Benliang, L., Lei, Y., and Li, Y. (2008). Characteristics of thrust structures in the northern Longmenshan front belt. *Acta Pet. Sinica* 29(5),657–662. doi:10.3321/j.issn:0253-2697.2008.05.005

Chen, Z., Li, W., Wang, L., Lei, Y., Yang, G., Zhang, B., et al. (2019). Structural geology and favorable exploration prospect belts in northwestern Sichuan basin, SW China. *Pet. Explor. Dev.* 46 (002), 413–425. doi:10.1016/s1876-3804(19)60022-4

Colletta, B., Letouzey, J., Pinedo, R., Ballard, J. F., and Balé, P. (1991). Computerized X-ray tomography analysis of sandbox models: examples of thin-skinned thrust systems. *Geology* 19 (11), 1063–1067. doi:10.1130/0091-7613(1991)019<1063:cxrtao>2.3.co;2

Cotton, J. T., and Koyi, H. A. (2000). Modeling of thrust fronts above ductile and frictional detachments: application to structures in the Salt Range and Potwar Plateau, Pakistan. *Geol. Soc. Am. Bull.* 112, 351–363. doi:10.1130/0016-7606(2000)112<351:motfad>2.0.co;2

Couzens-Schultz, B. A., Vendeville, B. C., and Wiltschko, D. V. (2003). Duplex style and triangle zone formation: insights from physical modeling. *J. Struct. Geol.* 25 (10), 1623–1644. doi:10.1016/S0191-8141(03)00004-X

Cui, J., Jia, D., Yin, H., Chen, Z., Li, Y., Wang, M., et al. (2020). The influence of a weak upper ductile detachment on the Longmen Shan fold-and-thrust belt (eastern margin of the Tibetan plateau): insights from sandbox experiments. *J. Asian Earth Sci.* 198, 104220. doi:10.1016/j.jseaes.2019.104220

Dahlen, F. A. (1990). Critical taper model of fold-and-thrust belts and accretionary wedges. *Annu. Rev. Earth Planet. Sci.* 18, 55–99. doi:10.1146/annurev.ea.18.050190.000415

Davis, D. M., and Engelder, T. (1985). The role of salt in fold-and-thrust belts. *Tectonophysics* 119 (1-4), 67–88. doi:10.1016/0040-1951(85)90033-2

Davis, D., Suppe, J., and Dahlen, F. A. (1983). Mechanics of fold-and-thrust belts and accretionary wedges. *J. Geophys. Res.* 88, 1153–1172. doi:10.1029/JB088iB02p01153

Fan, X., Jia, D., Yin, H., Shen, L., Liu, J., Cui, J., et al. (2020). Analogue modeling of the northern Longmen Shan thrust belt (eastern margin of the Tibetan plateau) and strain analysis based on particle image velocimetry. *J. Asian Earth Sci.* 198, 104238. doi:10.1016/j.jseaes.2020.104238

Feng, L., Bartholomew, M. J., and Choi, E. (2015). Spatial arrangement of décollements as a control on the development of thrust faults. *J. Struct. Geol.* 75, 49–59. doi:10.1016/j.jsg.2015.03.002

Gan, W., Zhang, P., Shen, Z. K., Niu, Z., Wang, M., Wan, Y., et al. (2007). Present-day crustal motion within the Tibetan Plateau inferred from GPS measurements. *J. Geophys. Res.* 112, 1–14. doi:10.1029/2005JB004120

Ghani, H., Gerold, Z., Sobel, E. R., and Ghasem, H. (2018). Structural variation within the himalayan fold and thrust belt: a case study from the Kohat-Potwar fold thrust belt of Pakistan. *J. Struct. Geol.* 116, 34–46. doi:10.1016/j.jsg.2018.07.022

Gong, L., Zeng, L., Gao, Z., Zhu, R., and Zhang, B. (2015). Reservoir characterization and origin of tight gas sandstones in the upper Triassic Xujiahe formation, western Sichuan basin, China. *J. Pet. Explor. Prod. Technol.* 6 (3), 319–329. doi:10.1007/s13202-015-0203-9

Graveleau, F., Malavieille, J., and Dominguez, S. (2012). Experimental modelling of orogenic wedges: a review. *Tectonophysics* 538-540, 1–66. doi:10.1016/j.tecto.2012.01.027

Gu, Z., Wang, X., Nunns, A., Zhang, B., and Zhai, X. (2020). Structural styles and evolution of a thin-skinned fold-and-thrust belt with multiple detachments in the eastern Sichuan Basin, south china. *J. Struct. Geol.* 104191. doi:10.1016/j.jsg.2020.104191

Guo, X., Gao, R., Randy Keller, G., Xu, X., Wang, H., and Li, W. (2013). Imaging the crustal structure beneath the eastern Tibetan plateau and implications for the uplift of the Longmen Shan range. *Earth Planet. Sci. Lett.* 379, 72–80. doi:10.1016/j.epsl.2013.08.005

He, W., Zhou, J., and Yuan, K. (2018). Deformation evolution of Eastern Sichuan-Xuefeng fold-thrust belt in South China: insights from analogue modelling. *J. Struct. Geol.* 109, 74–85. doi:10.1016/j.jsg.2018.01.002

Huang, G., Zhang, Z., Zhang, H., Huangfu, P., and Li, Z. H. (2020). Development of contrasting folding styles in the western Yangtze block, south China: insights from numerical modeling. *Tectonophysics* 792, 228579. doi:10.1016/j.tecto.2020.228579

Hubbard, J., and Shaw, J. H. (2009). Uplift of the longmen Shan and Tibetan plateau, and the 2008 wenchuan (M = 7.9) earthquake. *Nature* 458, 194–197. doi:10.1038/nature07837

Hubbard, J., Shaw, J. H., and Klinger, Y. (2010). Structural setting of the 2008 Mw 7.9 Wenchuan, China, earthquake. *Bull. Seismol. Soc. Am.* 100, 2713–2735. doi:10.1785/0120090341

Jaumé, S. C., and Lillie, R. J. (1988). Mechanics of the Salt Range-Potwar plateau, Pakistan: a fold-and-thrust belt underlain by evaporites. *Tectonics* 7 (1), 57–71. doi:10.1029/TC007i001p00057

Jia, D., Chen, Z. X., Jia, C. Z., Wei, G. Q., Zhang, Q., Wei, D. T., et al. (2003). Structural features of the Longmen Shan fold-and-thrust belt and development of the western Sichuan foreland basin, central China. *Geol. J. China Univ.* 9 (3), 402–410. doi:10.1016/S0955-2219(02)00073-0

Jia, D., Wei, G., Chen, Z., Benliang, L., Zen, Q., and Yang, G. (2006). Longmen Shan fold-thrust belt and its relation to the western Sichuan basin in central China: new insights from hydrocarbon exploration. *AAPG Bull.* 90, 1425–1447. doi:10.1306/03230605076

Jia, D., Li, Y., Lin, A., Wang, M., Chen, W., Wu, X., et al. (2010). Structural model of 2008 M_w 7.9 Wenchuan earthquake in the rejuvenated Longmen Shan thrust belt, China. *Tectonophysics* 491, 174–184. doi:10.1016/j.tecto.2009.08.040

Jia, D., Li, Y., Yan, B., Li, Z., and Zhang, Y. (2020). The Cenozoic thrusting sequence of the Longmen Shan fold-and-thrust belt, eastern margin of the Tibetan Plateau: insights from low-temperature thermochronology. *J. Asian Earth Sci.* 198, 104381. doi:10.1016/j.jseaes.2020.104381

Jin, W., Tang, L., Yang, K., Wan, G., and Lü, Z. (2010). Segmentation of the longmen mountains thrust belt, western sichuan foreland basin, SW China. *Tectonophysics* 485 (1–4), 107–121. doi:10.1016/j.tecto.2009.12.007

Klinkmüller, M., Schreurs, G., Rosenau, M., and Kemnitz, H. (2016). Properties of granular analogue model materials: a community wide survey. *Tectonophysics* 684, 23–38. doi:10.1016/j.tecto.2016.01.017

Koyi, H. A., Hessami, K., and Teixell, A. (2000). Epicenter distribution and magnitude of earthquakes in fold-thrust belts: insights from sandbox models. *Geophys. Res. Lett.* 27 (2), 273–276. doi:10.1029/1999GL010833

Krantz, R. W. (1991). Measurements of friction coefficients and cohesion for faulting and fault reactivation in laboratory models using sand and sand mixtures. *Tectonophysics* 188 (1), 203–207. doi:10.1016/0040-1951(91)90323-K

Li, Y., Allen, P. A., Densmore, A. L., and Xu, Q. (2003). Evolution of the longmen Shan foreland basin (western sichuan, China) during the late triassic indosinian orogeny. *Basin. Res.* 15(1), 117–138. doi:10.1046/j.1365-2117.2003.00197.x

Li, Y., Jia, D., Shaw, J. H., Hubbard, J., Lin, A., Wang, M., et al. (2010). Structural interpretation of the coseismic faults of the Wenchuan earthquake: three-dimensional modeling of the Longmen Shan fold-and-thrust belt. *J. Geophys. Res.* 115, B04317. doi:10.1029/2009JB006824

Li, Z. G. (2014). Late Cenozoic crustal shortening in Longmen Shan fold-and-thrust belt and tectonics stress field changes. PhD thesis. Nanjing, China: Nanjing Univeristy.

Li, Z. G., Jia, D., and Chen, W. (2013). Structural geometry and deformation mechanism of the Longquan anticline in the Longmen Shan fold-and-thrust belt, eastern Tibet. *J. Asian Earth Sci.* 64, 223–234. doi:10.1016/j.jseaes.2012.12.022

Li, Y., Jia, D., Wang, M., Shaw, J. H., He, J., Lin, A., et al. (2014). Structural geometery of the source region for the 2013 Mw 6.6 Lushan earthquake: implication for earthquake hazard assessment along the Longmen Shan. *Earth Planet. Sci. Lett.* 390, 275–286. doi:10.1016/j.epsl.2014.01.018

Li, Z. G., Liu-Zeng, J., Jia, D., Sun, C., Wang, W., Yuan, Z. D., et al. (2016). Quaternary activity of the range front thrust system in the Longmen Shan piedmont, China, revealed by seismic imaging and growth strata. *Tectonics* 35, 2807–2827. doi:10.1002/2015TC004093

Li, Z. G., Liu-Zeng, J., Almeida, R., Hubbard, J., Sun, C., and Yi, G. (2017). Re-evaluating seismic hazard along the southern Longmen Shan, China: insights

from the 1970 Dayi and 2013 Lushan earthquakes. *Tectonophysics* 717, 519–530. doi:10.1016/j.tecto.2017.09.001

Li, Y., Chen, S., Wang, Y., Su, K., He, Q., Qiu, W., et al. (2019a). Relationships between hydrocarbon evolution and the geochemistry of solid bitumen in the Guanwushan formation, NW Sichuan basin. *Mar. Pet. Geol.* 111, 116–134. doi:10.1016/j.marpetgeo.2019.08.018

Li, Y., Lu, R., He, D., Wang, X., Liu, Y., Xu, X., et al. (2019b). Transformation of coseismic faults in the northern Longmenshan tectonic belt, eastern Tibetan Plateau: implications for potential earthquakes and seismic risks. *J. Asian Earth Sci.* 177, 66–75. doi:10.1016/j.jseaes.2019.03.013

Li, Z., Zhang, P., Jia, D., Zheng, W., Sun, C., Li, Y., et al. (2019c). 3d geometric modeling for the Yanjinggou anticline in the Longmen Shan fold-and-thrust belt, China: oblique thrusting kinematic implications. *J. Asian Earth Sci.* 179, 99–111. doi:10.1016/j.jseaes.2019.04.005

Liang, H., Ran, Q., Di, G., Zeng, M., Han, S., and Wang, Y. (2019). Kink folds discovered in Qixia Formation of the buried structural belt, northwestern Sichuan Basin: their significance to oil and gas. *Nat. Gas Explor. Dev.* 42 (4), 1–7. doi:10.12055/gaskk.issn.1673-3177.2019.04.001

Liu, S. G., Luo, Z. L., Dai, S. L., Dennis, A., and Wilson, C. J. L. (1996). The uplift of the longmenshan thrust belt and subsidence of the west sichuan foreland basin. *Acta Geol. Sin.* 9, 16–26. doi:10.1111/j.1755-6724.1996.mp9001002.x

Liu, S. G., Deng, B., Li, Z. W., and Sun, W. (2012). Architecture of basin-mountain systems and their influences on gas distribution: a case study from the Sichuan basin, south China. *J. Asian Earth Sci.* 47, 204–215. doi:10.1016/j.jseaes.2011.10.012

Liu, S. G., Yang, Y., Deng, B., Zhong, Y., Wen, L., Sun, W., et al. (2020). Tectonic evolution of the Sichuan basin, southwest China. *Earth Sci. Rev.* 213, 103470. doi:10.1016/j.earscirev.2020.103470

Lohrmann, J., Kukowski, N., Adam, J., and Oncken, O. (2003). The impact of analogue material properties on the geometry, kinematics, and dynamics of convergent sand wedges. *J. Struct. Geol.* 25, 1691–1711. doi:10.1016/S0191-8141(03)00005-1

Lu, R., He, D., Suppe, J., Ma, Y., Liu, B., and Chen, Y. (2012). Along-strike variation of the frontal zone structural geometry of the central Longmen Shan thrust belt revealed by seismic reflection profiles. *Tectonophysics* 580, 178–189. doi:10.1016/j.tecto.2012.09.018

Lu, R., He, D., John, S., Wu, J. E., Liu, B., and Chen, Y. (2014). Structural model of the central Longmen Shan thrusts using seismic reflection profiles: implications for the sediments and deformations since the Mesozoic. *Tectonophysics* 630, 43–53. doi:10.1016/j.tecto.2014.05.003

Lu, R., He, D., Xu, X., and Liu, B. (2016). Crustal-scale tectonic wedging in the central Longmen Shan: constraints on the uplift mechanism in the southeastern margin of the Tibetan Plateau. *J. Asian Earth Sci.* 117 (March 1), 73–81. doi:10.1016/j.jseaes.2015.11.019

Lu, R., Xu, X., He, D., John, S., Liu, B., Wang, F., et al. (2017). Seismotectonics of the 2013 Lushan M_w 6.7 earthquake: inversion tectonics in the eastern margin of the Tibetan Plateau. *Geophys. Res. Lett.* 44 (16), 8236–8243. doi:10.1002/2017GL074296

Lu, R., He, D., Xu, X., Tan, X., Li, Y., Cai, M., et al. (2018). Geometry and kinematics of buried structures in the piedmont of the central Longmen Shan: implication for the growth of the eastern Tibetan Plateau. *J. Geol. Soc.* 176, 323–333. doi:10.1144/jgs2018-015

Luo, Z., and Long, X. (1992). Uplifting of the Longmen Shan orogenic zone and subsidence of western Sichuan foreland basin: Sichuan *Bull. Geol.* 12, 1–15.

María, L., Storti, F., Balanyá, J. C., Crespo-Blanc, A., and Rossetti, F. (2003). Role of décollement material with different rheological properties in the structure of the Aljibe thrust imbricate (flysch trough, Gibraltar arc): an analogue modelling approach. *J. Struct. Geol.* 25 (6), 867–881. doi:10.1016/S0191-8141(02)00087-1

Massoli, D., Koyi, H. A., and Barchi, M. R. (2006). Structural evolution of a fold-and-thrust belt generated by multiple décollements: analogue models and natural examples from the northern Apennines (Italy). *J. Struct. Geol.* 28 (2), 185–199. doi:10.1016/j.jsg.2005.11.002

Meng, Q. R., Wang, Erchie., and Hu, J. M. (2005). Mesozoic sedimentary evolution of the northwest Sichuan basin: implication for continued clockwise rotation of the South China block. *Geol. Soc. Am. Bull* 117, 396–410. doi:10.1130/B25407.1

Mount, V. S. (2014). Structural style of the Appalachian Plateau fold belt, north-central Pennsylvania. *J. Struct. Geol.* 69, 284–303. doi:10.1016/j.jsg.2014.04.005

Nilforoushan, F., Koyi, H. A., Swantesson, J. O. H., and Talbot, C. J. (2008). Effect of basal friction on surface and volumetric strain in models of convergent settings measured by laser scanner. *J. Struct. Geol.* 30 (3), 366–379. doi:10.1016/j.jsg.2007.09.013

Panien, M., Schreurs, G., and Pfiffner, A. (2006). Mechanical behaviour of granular materials used in analogue modelling: insights from grain characterisation, ring-shear tests and analogue experiments. *J. Struct. Geol.* 28 (9), 1710–1724. doi:10.1016/j.jsg.2006.05.004

Ramberg, H. (1981). *Gravity, deformation, and the Earth's crust in theory, experiments, and geological applications*. 2nd revised ed (London, United Kingdom: Academic).

Reber, J. E., Cooke, M. L., and Dooley, T. P. (2020). What model material to use? a review on rock analogs for structural geology and tectonics. *Earth Sci. Rev.* 202, 103107. doi:10.1016/j.earscirev.2020.103107

Ritter, M. C., Leever, K., Rosenau, M., and Oncken, O. (2016). Scaling the sandbox—mechanical (dis) similarities of granular materials and brittle rock. *J. Geophys. Res. Solid Earth* 121, 6863–6879. doi:10.1002/2016JB012915

Ruh, J. B., Kaus, B. J. P., and Burg, J. P. (2012). Numerical investigation of deformation mechanics in fold-and-thrust belts: influence of rheology of single and multiple décollements. *Tectonics* 31, TC3005. doi:10.1029/2011TC003047

Sak, P. B., McQuarrie, N., Oliver, B. P., Lavdovsky, N., and Jackson, M. S. (2012). Unraveling the central Appalachian fold-thrust belt, Pennsylvania: the power of sequentially restored balanced cross sections for a blind fold-thrust belt. *Geosphere* 8 (3), 685–702. doi:10.1130/GES00676.1

Sommaruga, A. (1999). Décollement tectonics in the Jura foreland fold-and-thrust belt. *Mar. Pet. Geol.* 16 (2), 111–134. doi:10.1016/S0264-8172(98)00068-3

Storti, F., Soto Marín, R., Rossetti, F., and Sainz, A. M. C. (2007). Evolution of experimental thrust wedges accreted from along-strike tapered, silicone-floored multilayers. *J. Geol. Soc.* 164 (1), 73–85. doi:10.1144/0016-76492005-186

Sun, C., Jia, D., Yin, H. W., Chen, Z. X., Li, Z. G., Shen, L., et al. (2016). Sandbox modeling of evolving thrust wedges with different preexisting topographic relief: implications for the Longmen Shan thrust belt, eastern Tibet. *J. Geophys. Res. Solid Earth* 121, 4591–4614. doi:10.1002/2016JB013013

Sun, C., Li, Z., Zheng, W., Jia, D., Zhang, D., Fan, X., et al. (2019). 3d geometry of range front blind ramp and its effects on structural segmentation of the southern Longmen Shan front, eastern Tibet. *J. Asian Earth Sci.* 181 (Sep.1), 103911.1–103911.16. doi:10.1016/j.jseaes.2019.103911

Tang, L. J., Yang, K. M., Jin, W. Z., Lü, Z. Z., and Yu, Y. X. (2008). Multi-level décollement zones and detachment deformation of Longmen Shan thrust belt, Sichuan basin, Southwest China. *Sci. China Earth Sci.* 51 (Suppl. II), 32–43. doi:10.1007/s11430-008-6014-9

Van Keken, P., Spiers, C., van den Berg, A., and Muyzert, E. (1993). The effective viscosity of rocksalt: implementation of steady-state creep laws in numerical models of salt diapirism. *Tectonophysics* 225, 457–476. doi:10.1016/0040-1951(93)90310-G

Wang, M., Jia, D., Shaw, J. H., Hubbard, J., Lin, A., Li, Y., et al. (2013a). Active fault-related folding beneath the alluvial terrace in the south Longmen Shan range front, Sichuan basin, China: implications for seismic hazard. *Bull. Seismol. Soc. Am.* 103 (4), 2369–2385. doi:10.1785/0120120188

Wang, M., Jia, D., Lin, A., Shen, L., Rao, G., and Li, Y. (2013b). Late Holocene activity and historical earthquakes of the Qiongxi thrust fault system in the southern Longmen Shan fold-and-thrust belt, eastern Tibetan Plateau. *Tectonophysics* 584, 102–113. doi:10.1016/j.tecto.2012.08.019

Wang, C. Y., Chen, H. L., Cheng, X. G., and Li, K. (2013c). Evaluating the role of syn-thrusting sedimentation and interaction with frictional detachment in the structural evolution of the SW Tarim basin, NW China: insights from analogue modeling. *Tectonophysics* 608, 642–652. doi:10.1016/j.tecto.2013.08.016

Wang, M., Jia, D., Shaw, J. H., Hubbard, J., Plesch, A., Li, Y., et al. (2014a). The 2013 Lushan earthquake: implications for seismic hazards posed by the Range Front blind thrust in the Sichuan Basin, China. *Geology* 42 (10), 915–918. doi:10.1130/G35809.1

Wang, L., Chen, Z., Li, B., Lei, Y., and Yan, S. (2014b). Structural characteristics of the northern Longmenshan fold-thrust belt and the favorable exploration areas, Sichuan basin, southwest China. *Pet. Explor. Dev.* 41 (5), 591–597. doi:10.1016/S1876-3804(14)60070-7

Wang, M., and Lin, A. (2017). Active thrusting of the Longquan Fault in the central Sichuan basin, China, and the seismotectonic behavior in the Longmen Shan fold-and-thrust belt. *J. Geophys. Res. Solid Earth* 122, 5639–5662. doi:10.1002/2016JB013391

Wang, R., Xu, Z., Santosh, M., Cai, Z., and Xu, X. (2019). Formation of Dabashan arcuate structures: constraints from Mesozoic basement deformation in south Qinling orogen, China. *J. Struct. Geol.* 118, 135–149. doi:10.1016/j.jsg.2018.10.014

Wang, M., Wang, F., Jiang, D., Yan, B., Chen, Z., and Song, G. (2020). Interactions between thin- and thick-skinned tectonics at the western Sichuan Basin, China. *Tectonophysics* 796, 228628. doi:10.1016/j.tecto.2020.228628

Wei, G., Chen, G., Du, S., Zhang, L., and Yang, W. (2008). Petroleum systems of the oldest gas field in China: neoproterozoic gas pools in the Weiyuan gas field, Sichuan basin. *Mar. Pet. Geol.* 25, 371–386. doi:10.1016/j.marpetgeo.2008.01.009

Weijermars, R., Jackson, M. P. A., and Vendeville, B. (1993). Rheological and tectonic modelling of salt province. *Tectonophysics* 217, 143–174. doi:10.1016/0040-1951(93)90208-2

Weijermars, R., and Schmeling, H. (1986). Scaling of Newtonian and non-Newtonian fluid dynamics without inertia for quantitative modelling of rock flow due to gravity (including the concept of rheological similarity). Phys. Earth Planet. *Inter.* 43, 316–330. doi:10.1016/0031-9201(86)90021-X

Wu, Z., Yin, H., Wang, X., Zhao, B., and Jia, D. (2014). Characteristics and deformation mechanism of salt-related structures in the western Kuqa depression, Tarim basin: insights from scaled sandbox modeling. *Tectonophysics* 612-613, 81–96. doi:10.1016/j.tecto.2013.11.040

Yan, D. P., Zhou, M. F., Li, S. B., and Wei, G. Q. (2011). Structural and geochronological constraints on the Mesozoic-Cenozoic tectonic evolution of the Longmen Shan thrust belt, eastern Tibetan Plateau. *Tectonics* 30, TC6005. doi:10.1029/2011TC002867

Yan, D. P., Xu, Y. B., Dong, Z. B., Qiu, L., Zhang, S., and Wells, M. (2016). Fault related fold styles and progressions in fold-thrust belts: insights from sandbox modeling. *J. Geophys. Res. Solid Earth* 121, 2087–2111. doi:10.1002/2015JB012397

Yan, D. P., Qiu, L., Wells, M. L., Zhou, M. F., Meng, X., Lu, S., et al. (2018). Structural and geochronological constraints on the early Mesozoic north Longmen Shan Thrust Belt: foreland fold-thrust propagation of the SW Qinling orogenic belt, northeastern Tibetan plateau. *Tectonics* 37, 4595–4624. doi:10.1029/2018TC004986

Yang, Y., Chen, C., Wen, L., Chen, X., Liang, H., Liu, R., et al. (2018). Characteristics of buried structures in the northern Longmenshan mountains and its significance to oil and gas exploration in the Sichuan Basin. *Nat. Gas Indus. B* 388, 8–15. doi:10.3787/j.issn.1000-0976.2018.08.002

Zhang, P. Z., Shen, Z., Wang, M., Gan, W., Bürgmann, R., Molnar, P., et al. (2004). Continuous deformation of the Tibetan plateau from global positioning system data. *Geology* 32, 809–812. doi:10.1130/G20554.1

Zhang, Z., Zhang, H., Wang, L., Cheng, H., Shi, Y., and Leroy, Y. M. (2018). Concurrent deformation in the Longmen Shan and the Sichuan Basin: a critical wedge captured by limit analysis. *Tectonics* 37, 283–304. doi:10.1002/2017TC004791

Zhang, Z., Zhang, H., Wang, L., Cheng, H., and Shi, Y. (2019). Late Cenozoic structural deformation and evolution of the central-southern Longmen Shan fold-and-thrust belt, China: insights from numerical simulations. *J. Asian Earth Sci.* 176, 88–104. doi:10.1016/j.jseaes.2019.01.026

Zhao, G. Z., Unsworth, M. J., Zhan, Y., Wang, L. F., and Zhang, J. H. (2012). Crustal structure and rheology of the Longmenshan and Wenchuan mw 7.9 earthquake epicentral area from magnetotelluric data. *Geology* 40 (12), 1139–1142. doi:10.1130/g33703.1

Zou, C., Yang, Z., Dai, J., Dong, D., Zhang, B., Wang, Y., et al. (2015). The characteristics and significance of conventional and unconventional Sinian–Silurian gas systems in the Sichuan basin, central China. *Mar. Pet. Geol.* 64, 386–402. doi:10.1016/j.marpetgeo.2015.03.005

Conflict of Interest: The authors declare that the research was conducted in the absence of any commercial or financial relationships that could be construed as a potential conflict of interest.